

World Journal of *Radiology*

World J Radiol 2022 February 28; 14(2): 30-54



MINIREVIEWS

- 30 Acute coronary syndrome on non-electrocardiogram-gated contrast-enhanced computed tomography
Yoshihara S

LETTER TO THE EDITOR

- 47 Diagnostic accuracy of thoracic imaging modalities for the detection of COVID-19
Dawit H, Absi M, Islam N, Ebrahimzadeh S, McInnes MDF
- 50 Comments on "Review of the role of diagnostic modalities and imaging findings in the COVID-19 pandemic"
Vulasala SSR, Gopireddy DR, Bhosale P, Virarkar MK

ABOUT COVER

Associate Editor of *World Journal of Radiology*, Matteo Bauckneht, MD, PhD, Assistant Professor, Department of Health Sciences, University of Genova and IRCCS Ospedale Policlinico San Martino, Genova 16132, Italy. matteo.bauckneht@hsanmartino.it

AIMS AND SCOPE

The primary aim of *World Journal of Radiology* (*WJR*, *World J Radiol*) is to provide scholars and readers from various fields of radiology with a platform to publish high-quality basic and clinical research articles and communicate their research findings online.

WJR mainly publishes articles reporting research results and findings obtained in the field of radiology and covering a wide range of topics including state of the art information on cardiopulmonary imaging, gastrointestinal imaging, genitourinary imaging, musculoskeletal imaging, neuroradiology/head and neck imaging, nuclear medicine and molecular imaging, pediatric imaging, vascular and interventional radiology, and women's imaging.

INDEXING/ABSTRACTING

The *WJR* is now abstracted and indexed in Emerging Sources Citation Index (Web of Science), PubMed, PubMed Central, China National Knowledge Infrastructure (CNKI), China Science and Technology Journal Database (CSTJ), and Superstar Journals Database. The 2021 edition of Journal Citation Reports® cites the 2020 Journal Citation Indicator (JCI) for *WJR* as 0.51.

RESPONSIBLE EDITORS FOR THIS ISSUE

Production Editor: *Ying-Yi Yuan*; Production Department Director: *Xu Guo*; Editorial Office Director: *Jia-Ping Yan*.

NAME OF JOURNAL

World Journal of Radiology

ISSN

ISSN 1949-8470 (online)

LAUNCH DATE

January 31, 2009

FREQUENCY

Monthly

EDITORS-IN-CHIEF

Thomas J Vogl

EDITORIAL BOARD MEMBERS

<https://www.wjgnet.com/1949-8470/editorialboard.htm>

PUBLICATION DATE

February 28, 2022

COPYRIGHT

© 2022 Baishideng Publishing Group Inc

INSTRUCTIONS TO AUTHORS

<https://www.wjgnet.com/bpg/gerinfo/204>

GUIDELINES FOR ETHICS DOCUMENTS

<https://www.wjgnet.com/bpg/GerInfo/287>

GUIDELINES FOR NON-NATIVE SPEAKERS OF ENGLISH

<https://www.wjgnet.com/bpg/gerinfo/240>

PUBLICATION ETHICS

<https://www.wjgnet.com/bpg/GerInfo/288>

PUBLICATION MISCONDUCT

<https://www.wjgnet.com/bpg/gerinfo/208>

ARTICLE PROCESSING CHARGE

<https://www.wjgnet.com/bpg/gerinfo/242>

STEPS FOR SUBMITTING MANUSCRIPTS

<https://www.wjgnet.com/bpg/GerInfo/239>

ONLINE SUBMISSION

<https://www.f6publishing.com>

Acute coronary syndrome on non-electrocardiogram-gated contrast-enhanced computed tomography

Shu Yoshihara

Specialty type: Radiology, Nuclear Medicine and Medical Imaging

Provenance and peer review: Invited article; externally peer reviewed.

Peer-review model: Single blind

Peer-review report's scientific quality classification

Grade A (Excellent): 0
Grade B (Very good): B
Grade C (Good): 0
Grade D (Fair): 0
Grade E (Poor): 0

P-Reviewer: Apiratwarakul K

Received: October 18, 2021

Peer-review started: October 18, 2021

First decision: December 10, 2021

Revised: December 14, 2021

Accepted: February 15, 2022

Article in press: February 15, 2022

Published online: February 28, 2022



Shu Yoshihara, Department of Diagnostic Radiology, Iwata City Hospital, Iwata 438-8550, Japan

Corresponding author: Shu Yoshihara, MD, PhD, Doctor, Department of Diagnostic Radiology, Iwata City Hospital, 512-3 Ookubo, Iwata 438-8550, Japan. shuy@hospital.iwata.shizuoka.jp

Abstract

It is not rare for acute coronary syndrome (ACS) patients to present with symptoms that are atypical, rather than chest pain. It is sometimes difficult to achieve a definitive diagnosis of ACS for such patients who present with atypical symptoms, normal initial biomarkers of myocardial necrosis, and normal or nondiagnostic electrocardiograms (ECGs). Although cardiac CT allows for assessments of coronary artery stenosis as well as myocardial perfusion defect in patients with suspected ACS, it requires ECG gating and is usually performed with high-performance multislice CT for highly probable ACS patients. However, several recent reports have stated that ACS is detectable by myocardial perfusion defects even on routine non-ECG-gated contrast-enhanced CT. A growing number of contrast-enhanced CT scans are now being performed in emergency departments in search of pathologies responsible for a patient's presenting symptoms. In order to avoid inappropriate management for this life-threatening event, clinicians should be aware that myocardial perfusion defect is more commonly detectable even on routine non-ECG-gated contrast-enhanced CT performed in search of other pathologies.

Key Words: Acute coronary syndrome; Non-ECG-gated CT; Computed tomography; Myocardial perfusion defect; Emergency department

©The Author(s) 2022. Published by Baishideng Publishing Group Inc. All rights reserved.

Core Tip: Definitive diagnosis of acute coronary syndrome (ACS) is sometimes difficult to achieve, especially in patients who present with atypical symptoms, normal initial biomarkers of myocardial necrosis, and normal or nondiagnostic electrocardiograms (ECGs). In order to avoid inappropriate management for this life-threatening event, clinicians should be aware that myocardial perfusion defect is more commonly detectable even on routine non-ECG-gated contrast-enhanced computed tomography performed in search of other pathologies. In this review, several essential points of image interpretation in diagnosing ACS on non-ECG-gated contrast-enhanced computed tomography has been described.

Citation: Yoshihara S. Acute coronary syndrome on non-electrocardiogram-gated contrast-enhanced computed tomography. *World J Radiol* 2022; 14(2): 30-46

URL: <https://www.wjgnet.com/1949-8470/full/v14/i2/30.htm>

DOI: <https://dx.doi.org/10.4329/wjr.v14.i2.30>

INTRODUCTION

Acute coronary syndrome (ACS) is a term used to refer to a range of conditions associated with acute myocardial ischemia and/or infarction, which are usually due to an abrupt reduction in the coronary blood flow[1]. Chest pain characteristics, specific associated symptoms, electrocardiogram (ECG) abnormalities, and the levels of serum biomarkers of myocardial necrosis are essential for a diagnosis of ACS[1]. However, rather than chest pain, some ACS patients present with atypical symptoms[2-4]. A review of over 430,000 patients from the National Registry of Myocardial Infarction II with confirmed acute myocardial infarction (AMI) showed that one-third presented at the hospital with no chest pain [2]. Patients such as these often present with symptoms including dyspnea alone, weakness, nausea and/or vomiting, palpitations, syncope, or cardiac arrest. The implications of absence of chest pain are important in terms of therapy and prognosis. The Registry report revealed that patients without chest pain were less likely to receive a diagnosis of a confirmed MI on admission, and were also less likely to receive thrombolytic therapy or primary percutaneous coronary intervention, and to undergo treatment with appropriate medical therapy. It is unsurprising that these differences were associated with increased in-hospital mortality[2]. Therefore, it is sometimes difficult to achieve a definitive diagnosis of ACS, especially for patients who present with atypical symptoms, normal initial biomarkers of myocardial necrosis, and normal or nondiagnostic ECGs. Even in the presence of acute coronary ischemia, women, diabetics, and the elderly are more likely to present with atypical symptoms, and caution is required in evaluating possible ACS[2,3]. The use of computed tomography (CT) in the emergency department (ED) has increased at a consistent exponential rate[5]. Due to their greater temporal and spatial resolution, current multi-slice computed tomography (MSCT) systems are capable of rapid scanning that renders non-ECG-gated images with fewer cardiac motion artifacts. Although imaging of various cardiac diseases is superior with ECG-gated MSCT images, typically there is sufficient information provided in non-ECG-gated MSCT images of the thorax or abdomen to identify a number of incidental cardiac abnormalities like myocardial perfusion defect (MPD) of the left ventricle which may be related to the patient's presenting symptoms[6]. Consequently, clinically unrecognized ACS cases identified on CT performed for the indication of other diseases are increasing, especially in the ED. In this article, we present clinically unrecognized several ACS cases detected on routine non-ECG-gated contrast-enhanced CT performed in the ED for discriminating other pathologies. Non-ECG-gated contrast-enhanced CT was performed using an 80-row MSCT scanner (Aquilion Prime, Toshiba Medical Systems, Tochigi, Japan). The scanning parameters were as follows: tube voltage, 120 kV; tube current, mA modulation technique with a noise index of 12 (maximum 500 mA); gantry rotation time, 350 ms; reconstruction slice thickness, 1mm. An intravenous bolus of nonionic contrast medium (55 kg < body weight; iopamidol 300 mg iodine/mL, 55 kg ≥ body weight; iopamidol 370 mg iodine/ml) was delivered through a vein in the arm with a flow rate of 3.3 mL/s. The dose of contrast medium was appropriately 600 mg I/kg of body weight, to a maximum of 100 mL. The scanning delay was calculated by monitoring the contrast values that increased to 150 Hounsfield units in the descending aorta as the region of interest (25-30 s after injection). A second scan was performed 120 s after injection. When focal decrease of the left ventricular myocardial enhancement was visually found, a region of interest was manually set to measure CT attenuation values of the normal and hypoperfused myocardium. MPD was defined as a decrease of 20 or more Hounsfield units compared with the adjacent normal enhanced myocardium.

CARDIAC COMPUTED TOMOGRAPHY AND ACS

Progress in the technical development of cardiac CT enables rapid, accurate imaging of the cardiovascular system. With cardiac CT, it is necessary to use either prospective or retrospective ECG gating to synchronize the CT image with the ECG. In both methods, the waveform of the ECG is used to coordinate image reconstruction with the heart's position in the chest[7]. Recently, a large body of evidence has been published supporting early assessment of coronary artery stenosis by cardiac CT as an accurate, safe, and efficient rapid diagnostic strategy for ED patients with low-intermediate risk acute chest pain[8-11]. As a result, the appropriate use criteria for cardiac CT designated detection of coronary artery stenosis by cardiac CT as appropriate for use in acute chest pain patients for whom the likelihood of ACS is low or intermediate[12]. Moreover, identification of regional subendocardial or transmural hypoattenuation of the myocardium in cardiac CT provides incremental diagnostic value to detect ACS [13]. Based on this novel evidence, the updated SCCT guidelines for the interpretation and reporting of coronary CT angiography have newly designated that myocardial CT enhancement patterns should be assessed during performance of cardiac CT[14].

NON-ELECTROCARDIOGRAM-GATED CONTRAST-ENHANCED CT AND ACS

Recently, several reports have been published that suggest non-ECG-gated contrast-enhanced CT can detect ACS with high diagnostic accuracy (Table 1)[15-19]. Mano *et al*[17] evaluated the frequency of MPD on non-ECG-gated contrast-enhanced CT performed with a 64-slice CT scanner, which was done to assess aortic dissection or pulmonary embolism in 154 patients who had been admitted to the ED with acute chest pain and/or back pain. MPD was detected in 43 patients, 26 (60%) of whom were ultimately diagnosed with AMI. In the remaining 111 patients without MPD, only 2 (2%) were ultimately diagnosed with AMI. They showed good diagnostic performance for MPD on non-ECG-gated contrast-enhanced CT in predicting AMI with a sensitivity of 93% and a specificity of 87%. Watanabe *et al*[18] evaluated the presence of MPD on non-ECG-gated contrast-enhanced CT using a 64-slice CT scanner in 23 patients who had been admitted to the ED with acute-onset chest pain and underwent emergent invasive coronary angiography. Of the 23 patients, 13 were diagnosed with ACS and the remaining 10 were diagnosed with other conditions. MPD was detected in 11 (85%) of the 13 ACS patients. They showed good diagnostic performance for MPD on non-ECG-gated contrast-enhanced CT in predicting ACS with a sensitivity of 85% and a specificity of 90%. In comparison with the other studies using non-ECG-gated contrast-enhanced arterial phase CT imaging for detecting ACS, Yamazaki *et al*[19] evaluated the ACS detection capability of using non-ECG-gated contrast-enhanced parenchymal phase CT imaging acquired with a 100-s scan delay. They showed good diagnostic performance for MPD visualized on non-ECG-gated contrast-enhanced CT during the parenchymal phase in predicting ACS with a sensitivity of 91% and a specificity of 93%. In non-ECG-gated contrast-enhanced CT, the normal myocardium is usually blurry because reconstructed images are a mixture of the systolic and diastolic phases. Indeed, cardiac motion artifacts are recognized to be the most important factor to degrade diagnostic performance on non-ECG-gated contrast-enhanced CT[19]. However, the frequency of false positive cases who were misjudged to have MPD without myocardial ischemia mainly due to cardiac motion artifacts was only 15%-20% in the previous reports[17,18]. In cases with ACS, decreased regional myocardial wall motion due to acute myocardial ischemia will contribute to reduced motion artifacts and sharp visualization of the myocardial border.

IMPORTANT POINTS OF IMAGE INTERPRETATION IN DETECTING ACS ON NON-ELECTROCARDIOGRAM-GATED CONTRAST-ENHANCED CT

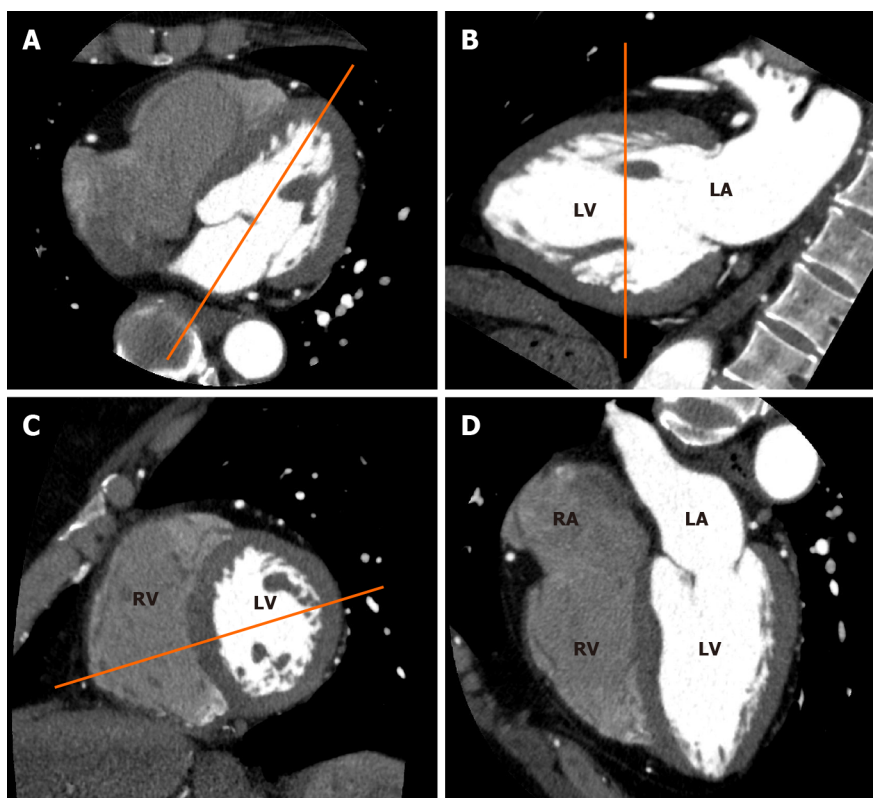
Vascular territories of the coronary artery

CT images are usually oriented and displayed using transaxial views, but these images do not cleanly transect the ventricle, atria, or myocardial regions supplied by the major coronary arteries. The American Heart Association (AHA) showed the cardiac plane definition and display for tomographic image modalities[20]. Essentially, it has been suggested that, using any noninvasive method, the displays for evaluation of cardiac structures are presented in three orthogonal cardiac planes: horizontal long axis, vertical long axis, and short axis (Figure 1). Therefore, it is important to evaluate a suspicious findings of MPD detected in transaxial images by multiplanar reformatted cardiac plane images. To identify a culprit coronary artery and likely location of flow-limiting coronary stenosis, knowledge of the distribution of coronary blood flow in the AHA 17-segment model of the left ventricle is also important. Figure 2 shows the general assignment of the 17 myocardial segments to one of the three major coronary arteries[20]. The apex, segment 17, which can be supplied by any of the three arteries, is where the greatest variability in myocardial blood supply occurs. Segments 1, 2, 7, 8, 13, 14, and 17 are assigned to the left anterior descending artery (LAD) distribution, and segments 3, 4, 9, 10, and 15 to the

Table 1 Studies investigating the ability of non-ECG-gated contrast-enhanced computed tomography to detect acute coronary syndrome

Ref.	Type of CT	CT phase	No. of Patients	No. of ACS	No. of positive MPD	True Positive	False Positive	True Negative	False Negative	Sensitivity (%)	Specificity (%)	PPV (%)	NPV (%)
Gosalia <i>et al</i> [15], 2004	SD	Arterial	37	18	16	15	1	18	3	83	95	94	86
Moore <i>et al</i> [16], 2006	16-slice	Arterial	87	11	10	6	4	72	5	55	95	60	94
Mano <i>et al</i> [17], 2015	64-slice	Arterial	154	28	43	26	17	109	2	93	87	60	98
Watanabe <i>et al</i> [18], 2016	64-slice	Arterial	23	13	12	11	1	9	2	85	90	92	82
Yamazaki <i>et al</i> [19], 2016	16/64-slice	Parenchymal	47	32	30	29	1	14	3	91	93	97	82

ACS: Acute coronary syndrome, MPD: Myocardial perfusion defect, PPV: Positive predictive value, NPV: Negative predictive value, SD: Single detector.



DOI: 10.4329/wjr.v14.i2.30 Copyright ©The Author(s) 2022.

Figure 1 Electrocardiogram-gated cardiac computed tomography (CT)-based sequential approach to CT imaging of cardiac planes. A: From an axial CT data set at the level of the mitral valve, a longitudinal plane bisecting the mitral valve and the left ventricular apex is used to create a vertical long axis view; **B:** From the vertical long axis view, a slice parallel to the mitral annulus at the mid ventricular level is used to obtain a short axis view; **C:** From the short axis view, a slice bisecting the center of the left ventricle (LV) and the intersection between the junction of the free wall and diaphragmatic wall of the right ventricle (RV) are used to obtain a horizontal long axis view. **(D)** Horizontal long axis view showing the left atrium, LV, right atrium and RV.

right coronary artery (RCA) when it is dominant. Generally, segments 5, 6, 11, 12, and 16 are assigned to the left circumflex coronary artery (LCX). However, it should be noted that the coronary artery blood supply to the myocardial segments is variable. Coronary dominance is determined by the artery supplying the posterior descending artery (Figure 3). Among the general population, approximately

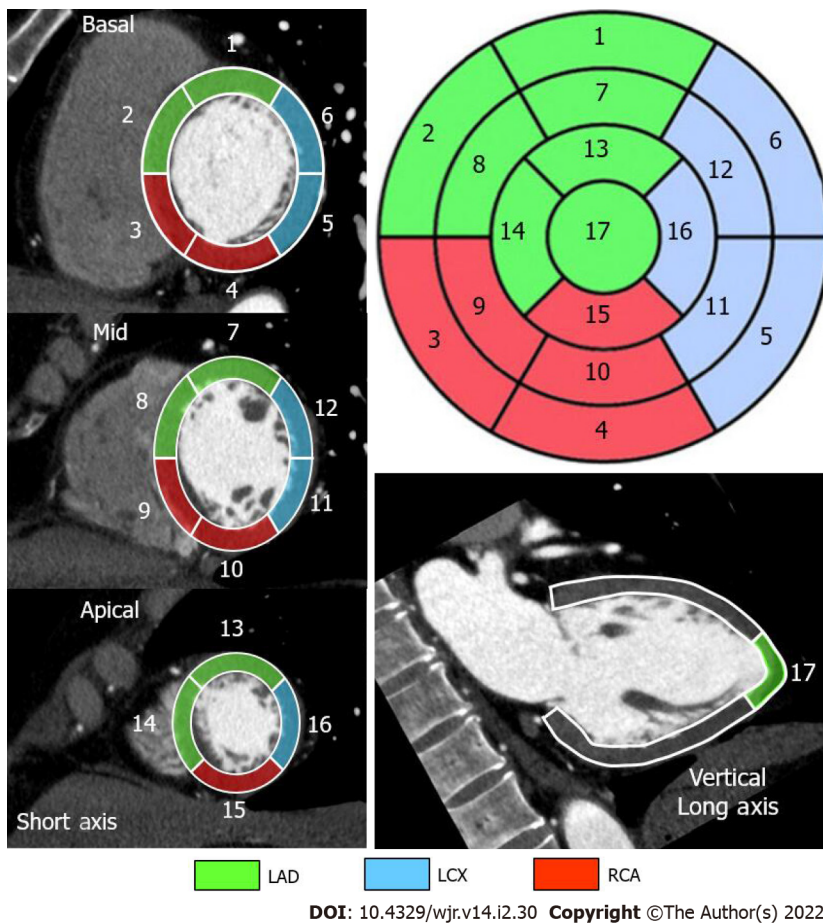


Figure 2 Standard segmental myocardial display in a 17-segment model. Electrocardiogram-gated cardiac computed tomography-based individual assignment of left ventricular segmentation following the American Heart Association 17-segment model with corresponding color-coded coronary artery perfusion territories for a right-dominant coronary system. LAD: Left anterior descending artery in green; LCX: Left circumflex coronary artery in blue; RCA: Right coronary artery in red.

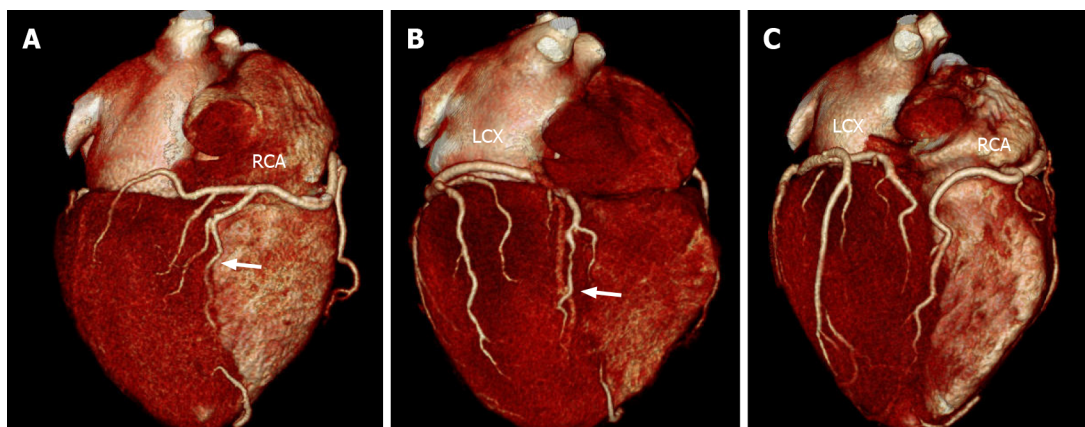
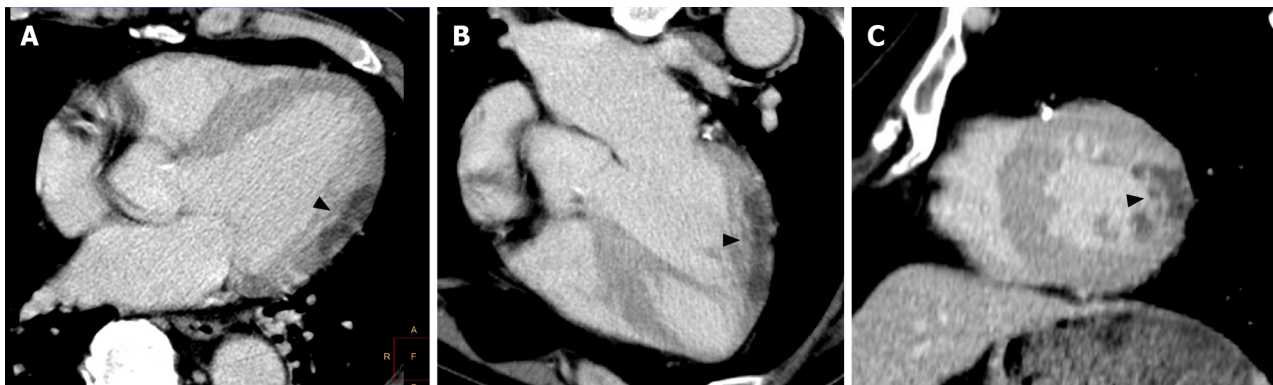


Figure 3 Variability in the coronary artery blood supply to the myocardium. Three-dimensional volume-rendered electrocardiogram-gated cardiac computed tomography images showing the inferior surface of the heart representing different coronary anatomy variants; A: Standard, right-dominant circulation. Right coronary artery (RCA) supplies posterior descending branch (arrow). Left circumflex coronary artery (LCX) supplies only inferolateral left ventricular myocardium; B: Left-dominant circulation. LCX supplies posterior descending branch (arrow). RCA supplies only right ventricular myocardium; C: Codominant circulation. Inferior myocardium is supplied both RCA and LCX.

70%-80% is right-dominant (supplied by the RCA), 5%-10% is left-dominant (supplied by the LCX), and 10%-20% is co-dominant (supplied by both the RCA and LCX)[21]. In our experience, MPD territories demonstrated on non-ECG-gated contrast-enhanced CT agree with the results of invasive coronary angiography, radionuclide myocardial perfusion imaging, and cardiac magnetic resonance imaging



DOI: 10.4329/wjr.v14.i2.30 Copyright ©The Author(s) 2022.

Figure 6 Non-electrocardiogram-gated contrast-enhanced computed tomography images in acute coronary syndrome of left circumflex coronary artery. A 65-year-old man with epigastralgia underwent non-electrocardiogram (ECG)-gated contrast-enhanced computed tomography (CECT) in search of aortic dissection. Axial (A), horizontal long axis (B), and short axis (C) reformatted non-ECG-gated CECT images acquired 120 s after contrast injection showed decreased myocardial enhancement in the mid lateral wall of the left ventricle (arrowheads).

with high accuracy (LAD: Figures 4 and 5, LCX: Figures 6 and 7, RCA: Figures 8 and 9).

Global myocardial ischemia

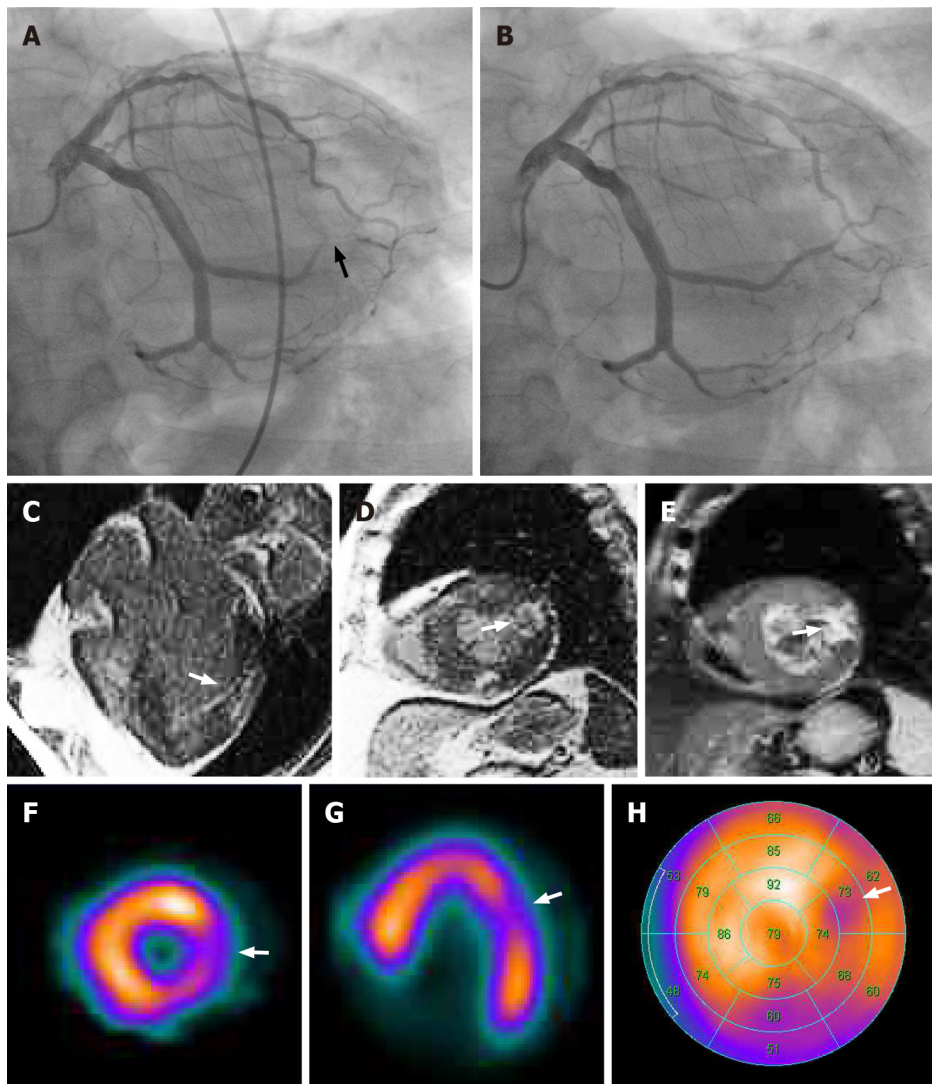
In a study that evaluated the presence of MPD on non-ECG-gated contrast-enhanced CT, Watanabe *et al* [18] described a patient with AMI of the left main trunk who did not show MPD. In our experience, broad MPD induced by the occlusion of the left main trunk highlights the normally perfused myocardial enhancement in the RCA territory (Figures 10 and 11). Balanced ischemia is a well-known limitation of stress radionuclide myocardial perfusion imaging[22]. MPD seen in radionuclide myocardial perfusion imaging results from the relative difference in radiotracer uptake of the left ventricular myocardium normalized to the most normal area with the highest radiotracer uptake. Therefore, in patients with ischemia that is relatively balanced among the three major vascular territories, this potentially results in a homogeneous radiotracer distribution in the myocardium, thus underestimating the severity of ischemia or even indicating a falsely normal result. MPD demonstrated on contrast-enhanced CT also reflects the relative difference in left ventricular myocardial contrast enhancement. Hence, it may be difficult to detect global myocardial ischemia as focal MPD on non-ECG-gated contrast-enhanced CT even in a rest condition.

Hemopericardium

Common causes of pericardial effusion include heart failure, renal failure, neoplasm, infection, and injury, including trauma and myocardial infarction[23]. Pericardial fluid characteristics are reflected in the CT attenuation value. It is likely that a value closer to the value of water (0 Hounsfield units) is a simple effusion. A value greater than that of water density can be observed in conditions including malignancy, purulent exudate, and hemopericardium[23]. Hemopericardium is induced by cardiac rupture, ruptured ascending aortic dissection, trauma, neoplasm, and as a consequence of cardiac surgery (iatrogenic)[24,25]. Left ventricular free wall rupture is one of the complications of AMI that is often fatal. Acute rupture is usually fatal, but some patients with a small ventricular tear, which may be sealed temporarily by a clot or fibrinous pericardial adhesions, may progress to a subacute form allowing late survival. In cases with hemopericardium, the presence of MPD on contrast-enhanced CT is a finding highly suspicious of left ventricular free wall rupture and should be carefully checked. Accompanying myocardial defects are also detected even in non-ECG-gated contrast-enhanced CT (Figures 12 and 13).

Papillary muscle

The papillary muscles are one of the components of the mitral valve apparatus[26]. Two papillary muscles arise from the area between the apical and middle thirds of the left ventricular wall. Both the anterior and posterior mitral valve leaflets are attached *via* primary, secondary, and tertiary chordae to both anterolateral and posteromedial papillary muscles. The anterolateral papillary muscle is often composed of a single major muscle group, whereas the posteromedial papillary muscle usually comprises two or three major muscle groups (Figure 14). Left ventricular papillary muscles are particularly vulnerable to ischemia because they are perfused by the terminal portion of the coronary vascular bed. The anterolateral papillary muscle is supplied by the diagonal branches of the LAD and often by marginal branches from the LCX. In contrast, the supply to the posteromedial papillary muscle is *via* the posterior descending branch of the LCX or RCA (depending on dominance)[27]. Necrosis of a papillary muscle is a frequent complication of MI and it should be recognized because it may lead to papillary



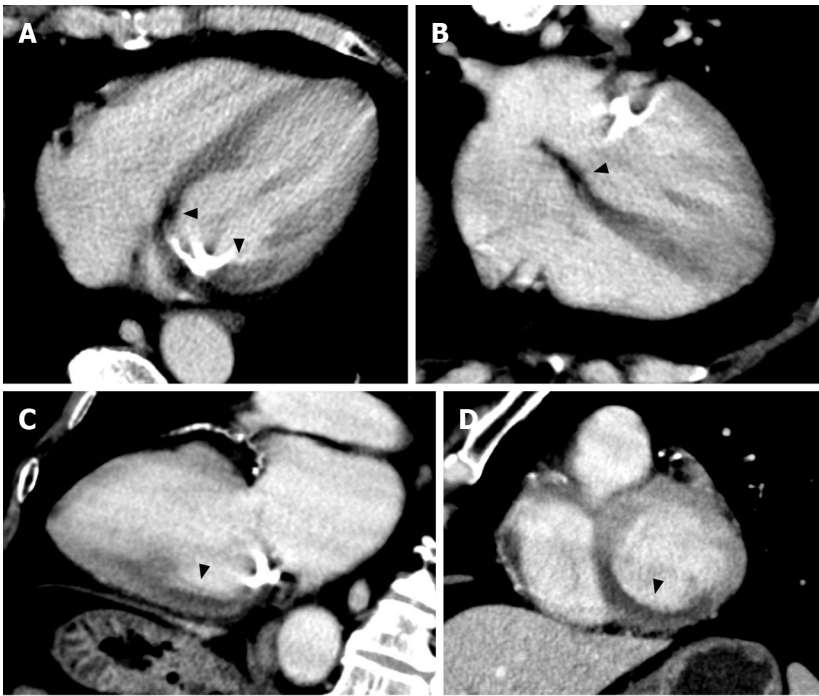
DOI: 10.4329/wjr.v14.i2.30 Copyright ©The Author(s) 2022.

Figure 7 Corresponding invasive coronary angiography, cardiac magnetic resonance imaging and tetrofosmin single-photon emission computed tomography in acute coronary syndrome of left circumflex coronary artery. Same patient as Figure 6. A: Invasive coronary angiography showed 99% stenosis in the posterolateral branch of the left circumflex coronary artery (arrow). B: Subsequent percutaneous coronary intervention was performed by balloon angioplasty and stent implantation. His laboratory data showed elevation of cardiac biomarkers (creatin kinase 1620 IU/L, creatine kinase MB 120 IU/L). Horizontal long axis (C) and short axis (D) views of the contrast-enhanced cardiac magnetic resonance imaging (MRI) showed late gadolinium enhancement in the mid lateral wall of the left ventricle (arrow). A short axis view of the T2-weighted cardiac MRI showed high signal intensity in the mid lateral wall of the left ventricle (E, arrow). Short axis (F) and horizontal long axis (G) views and a bull's eye polar plot (H) of rest technetium-99m tetrofosmin single-photon emission computed tomography myocardial perfusion imaging showed hypoperfusion in the mid lateral wall of the left ventricle (arrows).

muscle rupture, which is a rare but often-fatal mechanical complication. The posteromedial papillary muscle is particularly vulnerable to myocardial ischemia because of its single system of blood supply (Figure 15). The presence of MPD of the papillary muscle on contrast-enhanced CT is a finding suspicious of papillary muscle ischemia or necrosis, and detectable even in non-ECG-gated contrast-enhanced CT (Figure 16).

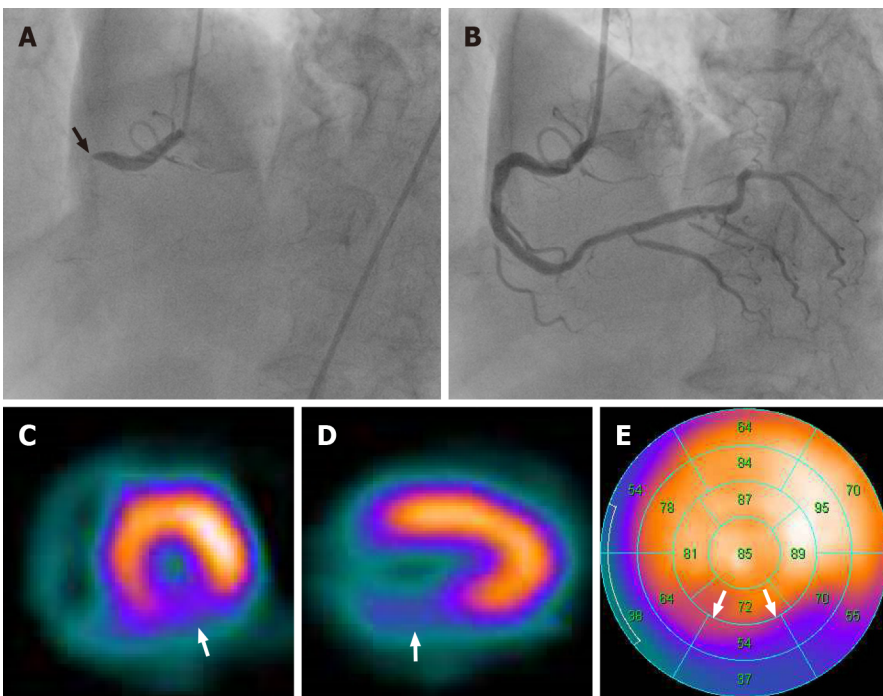
Myocardial fat

CT attenuation values are quantitative, and they can be used to define a structure's density or the iodine content after administration of iodinated contrast media. In a cardiac CT study, Nieman *et al*[28] showed that CT attenuation values found in patients with long-standing (over 1 year) MI (-13 ± 37 HU) were significantly lower than in patients with acute (within 1 wk) MI (26 ± 26 HU) and normal hearts (73 ± 14 HU). Histologic analyses showed that myocardial fat at the site of a healed MI is common with a prevalence of 68%-84% [29,30]. The presence of myocardial fat can be identified at the macroscopic level by CT, although a small amount of microscopic myocardial fat may be undetectable [31]. Myocardial fat at the site of a MI is frequently observed as a subendocardial low attenuation in the distribution of the culprit coronary artery on both non-contrast and contrast-enhanced CT even in non-ECG-gated CT (Figure 17). Concomitant regional myocardial wall motion reduction in areas of old MI may support the



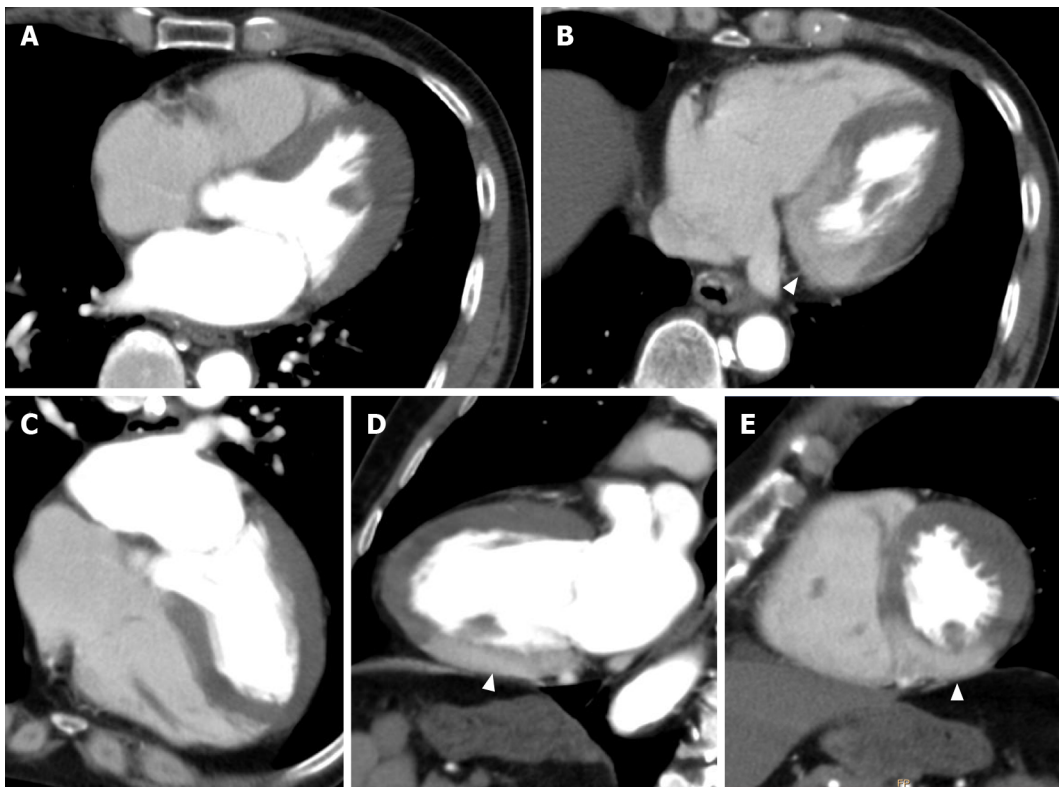
DOI: 10.4329/wjr.v14.i2.30 Copyright ©The Author(s) 2022.

Figure 8 Non-electrocardiogram-gated contrast-enhanced computed tomography images in acute coronary syndrome of right coronary artery. A 67-year-old man with chest pain underwent non-electrocardiogram (ECG)-gated contrast-enhanced computed tomography (CECT) in search of aortic dissection. Axial (A), horizontal long axis (B), vertical long axis (C), and short axis (D) reformatted non-ECG-gated CECT images acquired 120 s after contrast injection showed decreased myocardial enhancement in the basal to mid inferior, inferolateral, and inferoseptal wall of the left ventricle (arrowheads).



DOI: 10.4329/wjr.v14.i2.30 Copyright ©The Author(s) 2022.

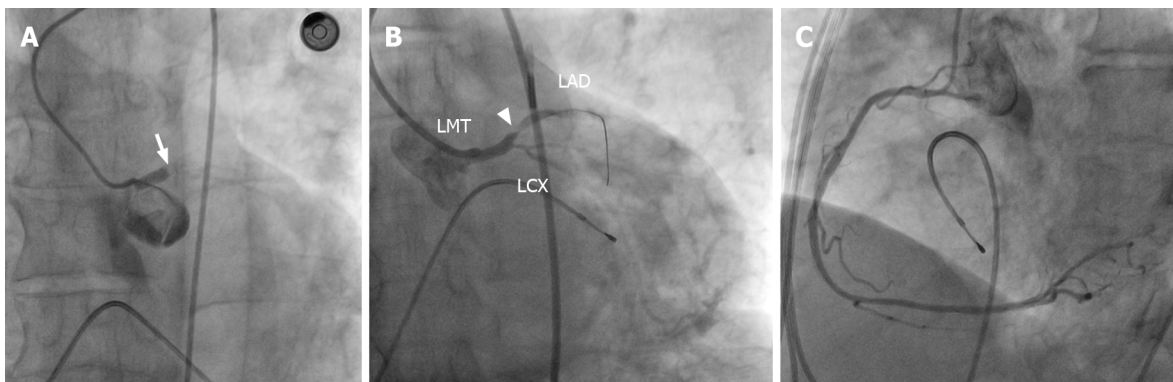
Figure 9 Corresponding invasive coronary angiography and sestamibi single-photon emission computed tomography in acute coronary syndrome of right coronary artery. Same patient as Figure 8. A: Invasive coronary angiography showed total occlusion in the proximal site of the right coronary artery (arrow); B: Subsequent percutaneous coronary intervention was performed by balloon angioplasty and stent implantation. His laboratory data showed elevation of cardiac biomarkers (creatinine kinase 1620 IU/L, creatine kinase MB 239 IU/L). Short axis (C) and vertical long axis (D) views and a bull's eye polar plot (E) of rest technetium-99m sestamibi single-photon emission computed tomography myocardial perfusion imaging showed perfusion defect in the basal to mid inferior, inferolateral and inferoseptal wall of the left ventricle (arrows).



DOI: 10.4329/wjr.v14.i2.30 Copyright ©The Author(s) 2022.

Figure 10 Non-electrocardiogram-gated contrast-enhanced computed tomography images in acute coronary syndrome of left main trunk.

A 70-year-old man with severe dyspnea underwent non-electrocardiogram (ECG)-gated contrast-enhanced computed tomography (CECT) for discriminating acute pulmonary thromboembolism. Axial (A, B), horizontal long axis (C), vertical long axis (D), and short axis (E) reformatted non-ECG-gated CECT images acquired 120 s after contrast injection showed localized myocardial enhancement only in the basal to mid inferior wall of the left ventricle (arrowheads).



DOI: 10.4329/wjr.v14.i2.30 Copyright ©The Author(s) 2022.

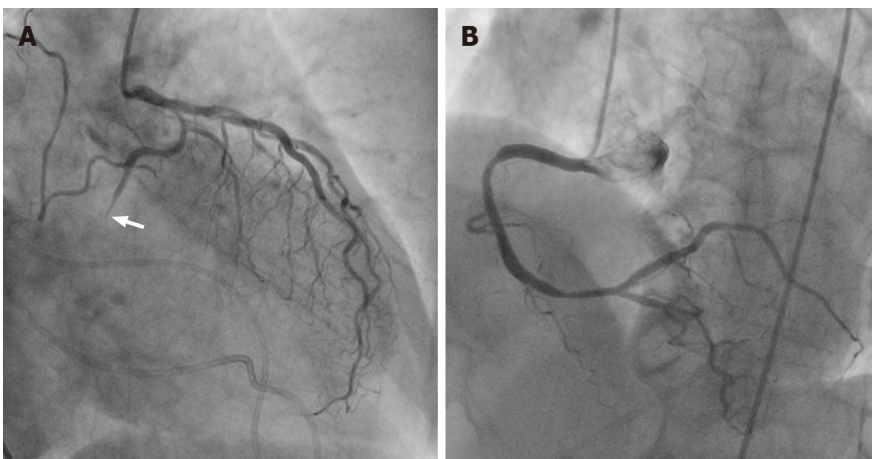
Figure 11 Corresponding invasive coronary angiography in acute coronary syndrome of left main trunk. Same patient as Figure 10. A: Invasive coronary angiography showed thrombotic occlusion in the left main trunk (arrow). Subsequent percutaneous coronary intervention (PCI) was tried. B: After guidewire was crossed to the left anterior descending artery, there was minimal improvement in flow and 99% stenosis in the proximal site of the left anterior descending artery appeared (arrowhead); C: The right coronary artery showed no significant stenosis. The patient died during PCI because of uncontrollable ventricular fibrillation. LMT: Left main trunk; LAD: Left anterior descending artery; LCX: Left circumflex coronary artery.

clear visualization of the myocardial fat. The prevalence of left ventricular myocardial fat detected by CT increases as the infarct age becomes higher[32]. Because it is important to differentiate ACS from OMI, in cases who present MPD on contrast-enhanced CT, CT-detectable myocardial fat associated with old MI should be excluded by comparison with non-contrast CT. In our experience, AMI of the RCA complicated with old MI of the diagonal branch was successfully distinguished by comparison with non-contrast CT in a non-ECG-gated CT examination (Figures 17-19). However, because OMI does not always show myocardial fat, it is difficult to differentiate ACS from OMI without CT-detectable myocardial fat only with usual contrast-enhanced computed tomography.



DOI: 10.4329/wjr.v14.i2.30 Copyright ©The Author(s) 2022.

Figure 12 Non-electrocardiogram-gated contrast-enhanced computed tomography images in postinfarct cardiac free wall rupture. A: An 81-year-old man with syncope first underwent non-electrocardiogram (ECG)-gated non-contrast whole body computed tomography (CT), and moderate pericardial effusion was found. The attenuation value of the pericardial effusion was about 50 Hounsfield units. Subsequently, non-ECG-gated contrast-enhanced CT (CECT) was performed in search of ascending aortic dissection. Axial (B), short axis (C), and horizontal long axis (D) reformatted non-ECG-gated CECT images acquired 120 s after contrast injection showed decreased myocardial enhancement in the basal to mid lateral wall of the left ventricle (arrowheads) and a small myocardial defect (arrow).

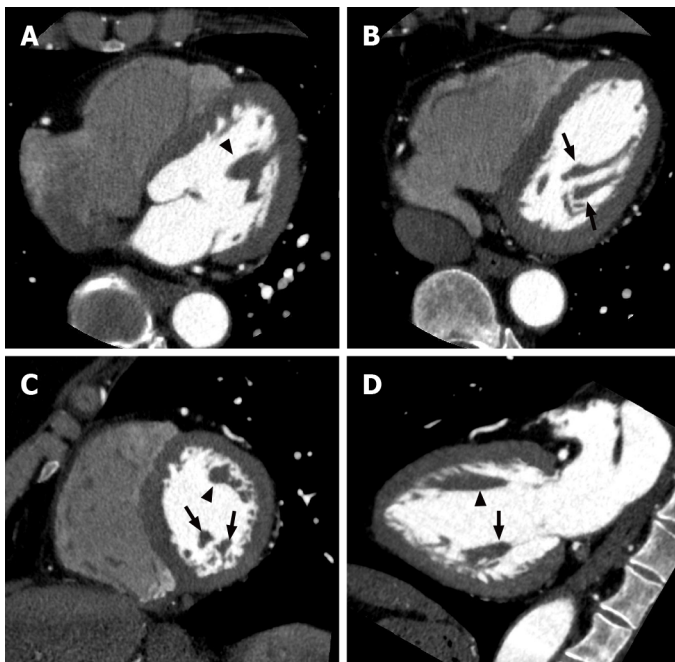


DOI: 10.4329/wjr.v14.i2.30 Copyright ©The Author(s) 2022.

Figure 13 Corresponding invasive coronary angiography in postinfarct cardiac free wall rupture. Same patient as Figure 12. A: Invasive coronary angiography showed total occlusion in the distal site of the left circumflex coronary artery (arrow); B: The right coronary artery showed no significant stenosis. The patient subsequently underwent a surgical operation. After removal of the large clot within the pericardium, a small perforation was found in the lateral wall of the left ventricle, confirming a definitive diagnosis of left ventricular free wall rupture.

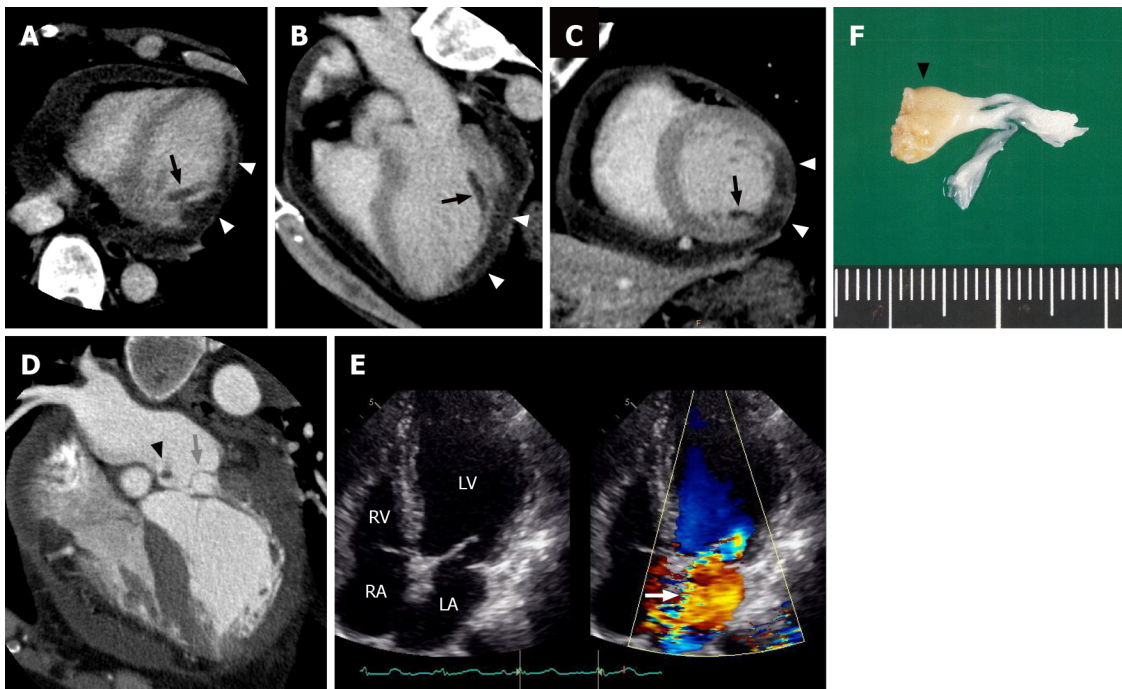
CONCLUSION

Definitive diagnosis of ACS is sometimes difficult to achieve, especially in patients who present with atypical symptoms, normal initial biomarkers of myocardial necrosis, and normal or nondiagnostic ECGs. In order to avoid inappropriate management for this life-threatening event, clinicians should be



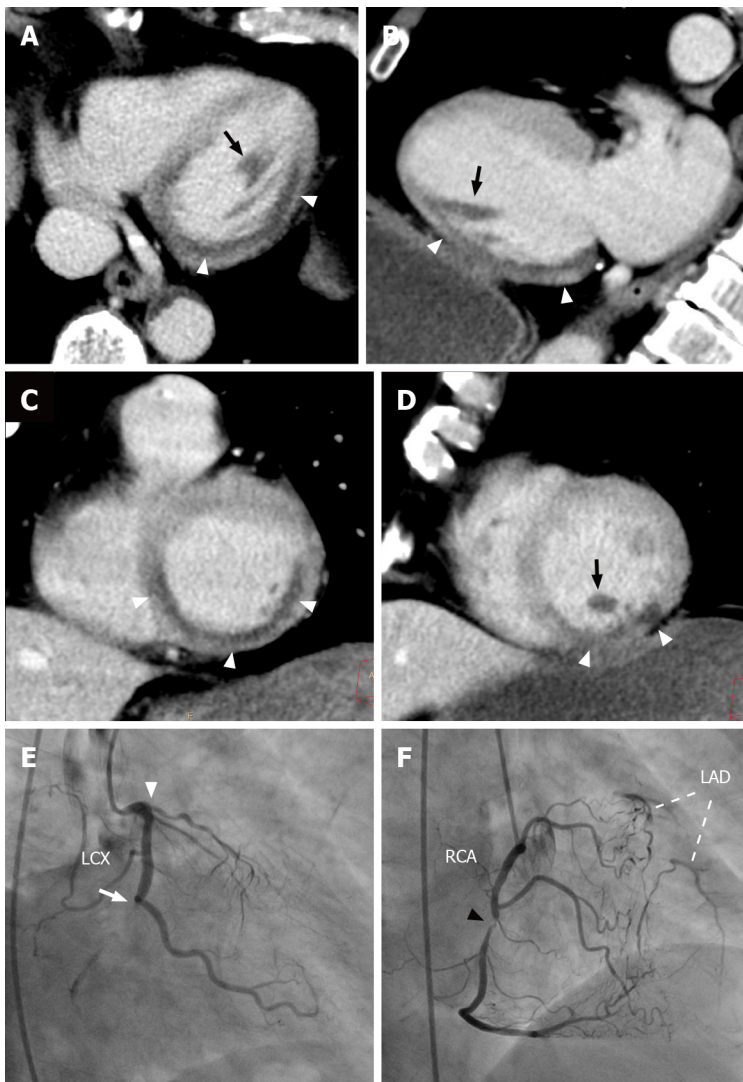
DOI: 10.4329/wjr.v14.i2.30 Copyright ©The Author(s) 2022.

Figure 14 Left ventricular papillary muscles. Axial (A, B), short axis (C), and vertical long axis (D) reformatted electrocardiogram-gated cardiac CT images showing the anatomy of the left ventricular chamber of the normal heart. The anterolateral (arrowheads) and posteromedial (arrows) papillary muscles manifest as filling defects within the contrast-filled left ventricular lumen.



DOI: 10.4329/wjr.v14.i2.30 Copyright ©The Author(s) 2022.

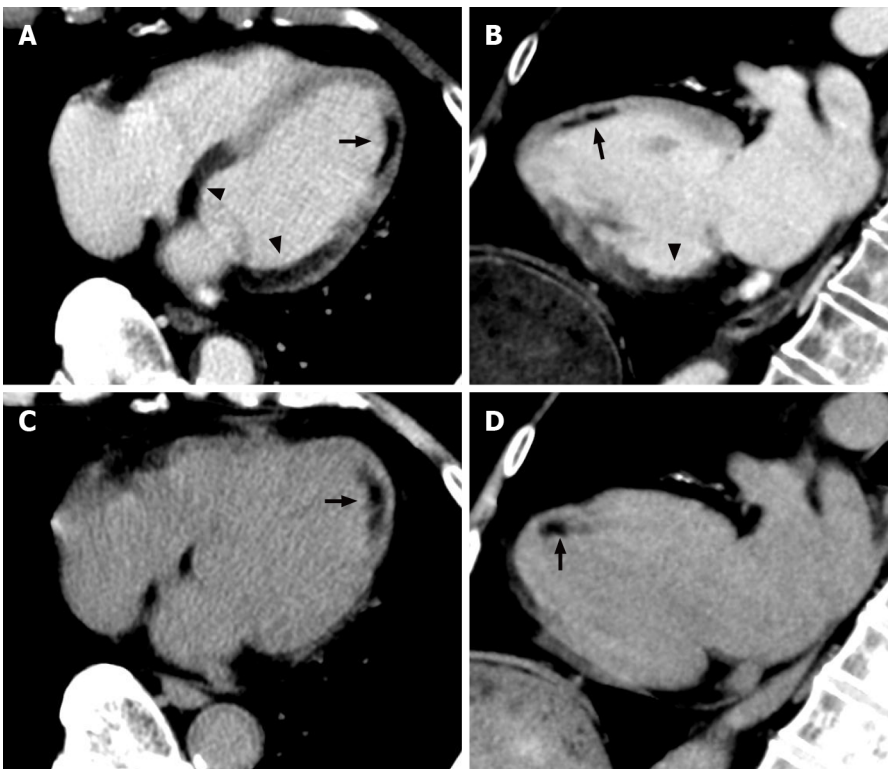
Figure 15 Postinfarct left ventricular papillary muscle rupture. Electrocardiogram-gated cardiac CT images from a 61-year-old man with posteromedial papillary muscle rupture complicated by acute ST elevation myocardial infarction due to total occlusion of the left circumflex coronary artery. Axial (A), three-chamber (B), and short axis (C) reformatted cardiac CT images showed decreased myocardial enhancement in the inferolateral wall (white arrowheads) and posteromedial papillary muscle (black arrows) of the left ventricle. A horizontal long axis image (D) showed severe prolapse of the posterior mitral valve leaflet into the left atrium (grey arrow) with discernible papillary muscle attachment (black arrowhead). An apical four-chamber color Doppler image of the transthoracic echocardiogram showed severe mitral regurgitation during ventricular systole extending to the posterior left atrial wall (E, white arrow). The patient subsequently underwent a mitral valve replacement. Surgical specimen showed posteromedial papillary muscle attached to the resected posterior mitral leaflet (F, black arrowhead). LV: Left ventricle; LA: Left atrium; RV: Right ventricle; RA: Right atrium.



DOI: 10.4329/wjr.v14.i2.30 Copyright ©The Author(s) 2022.

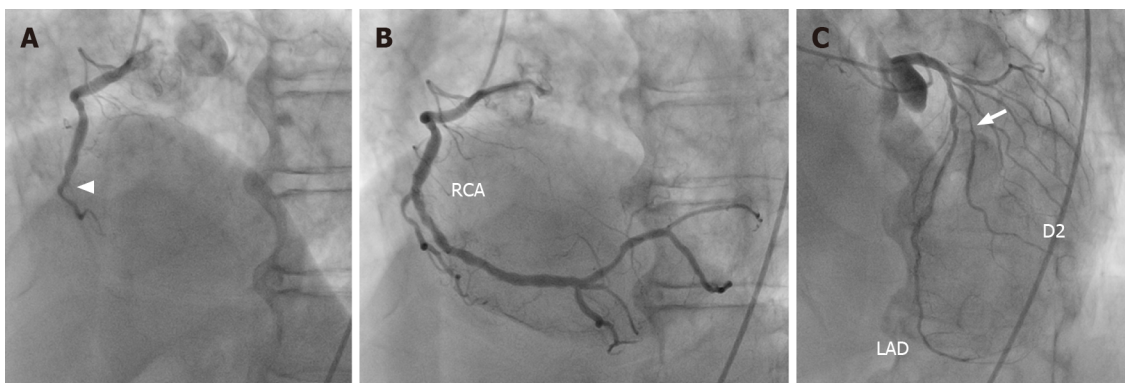
Figure 16 Myocardial perfusion defect of the posteromedial papillary muscle on non-electrocardiogram-gated contrast-enhanced computed tomography. A 68-year-old man with right anterior chest pain underwent non-electrocardiogram (ECG)-gated contrast-enhanced computed tomography (CECT) in search of aortic dissection. Axial (A), vertical long axis (B), and short axis (C, D) reformatted non-ECG-gated CECT images acquired 120 s after contrast injection showed decreased myocardial enhancement in the basal to mid inferior, inferolateral, and inferoseptal walls of the left ventricle (arrowheads). Decreased myocardial enhancement was also recognized in the posteromedial papillary muscle (arrows). Invasive coronary angiography showed total occlusion in the distal site of the left circumflex coronary artery (E, arrow), total occlusion in the proximal site of the left anterior descending artery (E, arrowhead), and 90% stenosis in the mid site of the right coronary artery (F, arrowhead), which provides abundant collateral flow to the left anterior descending artery. The patient subsequently underwent an emergent coronary artery bypass grafting. LAD: Left anterior descending artery; LCX: Left circumflex coronary artery; RCA: Right coronary artery.

aware that MPD is more commonly detectable even on routine non-ECG-gated contrast-enhanced CT performed in search of other pathologies.



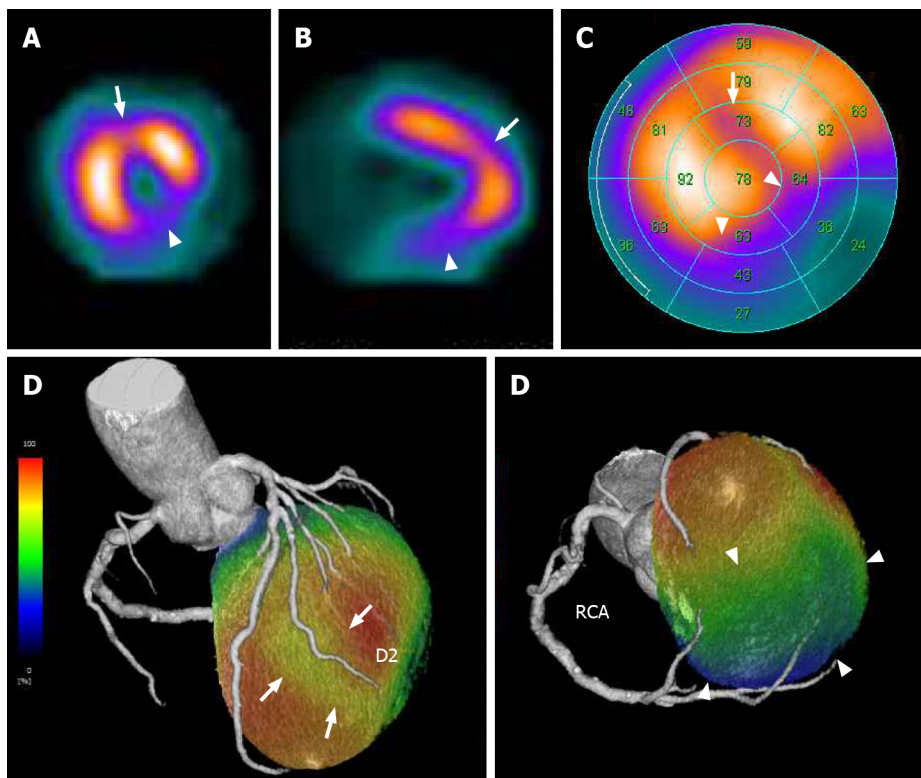
DOI: 10.4329/wjr.v14.i2.30 Copyright ©The Author(s) 2022.

Figure 17 Non-electrocardiogram-gated contrast-enhanced computed tomography images in acute coronary syndrome of right coronary artery complicated with anterior old myocardial infarction. An 82-year-old man with back pain underwent non-electrocardiogram (ECG)-gated contrast-enhanced computed tomography (CECT) in search of aortic dissection. Axial (A) and vertical long axis (B) reformatted non-ECG-gated CECT images acquired 120 s after contrast injection showed decreased myocardial enhancement in the basal to mid inferior, inferolateral, and inferoseptal walls of the left ventricle (arrowheads). Non-ECG-gated CECT images also showed decreased myocardial enhancement in the mid anterior wall of the left ventricle apart from the above-mentioned area (arrow). Axial (C) and vertical long axis (D) reformatted non-ECG-gated non-contrast CT images showed subendocardial low attenuation less than 0 Hounsfield units only in the mid anterior wall of the left ventricle, which is consistent with myocardial fatty degeneration associated with the old myocardial infarction (arrow).



DOI: 10.4329/wjr.v14.i2.30 Copyright ©The Author(s) 2022.

Figure 18 Corresponding invasive coronary angiography in acute coronary syndrome of right coronary artery complicated with anterior old myocardial infarction. Same patient as Figure 17. A: Invasive coronary angiography showed total occlusion in the mid site of the right coronary artery (arrowhead); B: Subsequent percutaneous coronary intervention was performed by balloon angioplasty and stent implantation. C: Invasive coronary angiography also showed 75% stenosis in the proximal site of the second diagonal branch (arrow). RCA: Right coronary artery; LAD: Left anterior descending artery; D2: Second diagonal branch.



DOI: 10.4329/wjr.v14.i2.30 Copyright ©The Author(s) 2022.

Figure 19 Corresponding sestamibi single-photon emission computed tomography in acute coronary syndrome of right coronary artery complicated with anterior old myocardial infarction. Same patient as Figures 17 and 18. Rest technetium-99m sestamibi single-photon emission computed tomography (SPECT) myocardial perfusion imaging (MPI) are shown. Short axis (A) and vertical long axis (B) views and a bull's eye polar plot (C) of rest technetium-99m sestamibi SPECT MPI showed perfusion defects in the basal to mid inferior, inferolateral, and inferoseptal walls of the left ventricle (arrowheads). In addition, SPECT MPI also showed hypoperfusion in the mid anterior wall of the left ventricle (arrows). The volume-rendered, coregistered SPECT MPI, and cardiac CT images demonstrated that hypoperfusion in the mid anterior wall of the left ventricle seen on the SPECT MPI corresponded with the territory of the second diagonal branch (D, arrows), whereas the perfusion defects in the basal to mid inferior, inferolateral, and inferoseptal walls of the left ventricle seen on the SPECT MPI corresponded with the territory of the right coronary artery (D, arrowheads). LAD: Left anterior descending artery, D2: Second diagonal branch; RCA: Right coronary artery.

FOOTNOTES

Author contributions: Yoshihara S designed and performed all of this study and wrote the all of the revised manuscript.

Conflict-of-interest statement: The authors declare that they have no conflicts of interest.

Open-Access: This article is an open-access article that was selected by an in-house editor and fully peer-reviewed by external reviewers. It is distributed in accordance with the Creative Commons Attribution NonCommercial (CC BY-NC 4.0) license, which permits others to distribute, remix, adapt, build upon this work non-commercially, and license their derivative works on different terms, provided the original work is properly cited and the use is non-commercial. See: <https://creativecommons.org/licenses/by-nc/4.0/>

Country/Territory of origin: Japan

ORCID number: Shu Yoshihara 0000-0001-9294-3767.

S-Editor: Liu JH

L-Editor: A

P-Editor: Liu JH

REFERENCES

- 1 **Amsterdam EA, Wenger NK, Brindis RG, Casey DE Jr, Ganiats TG, Holmes DR Jr, Jaffe AS, Jneid H, Kelly RF, Kontos MC, Levine GN, Liebson PR, Mukherjee D, Peterson ED, Sabatine MS, Smalling RW, Zieman SJ; ACC/AHA Task Force Members.** 2014 AHA/ACC guideline for the management of patients with non-ST-elevation acute coronary syndromes: a

- report of the American College of Cardiology/American Heart Association Task Force on Practice Guidelines. *Circulation* 2014; **130**: e344-e426 [PMID: 25249585 DOI: 10.1161/CIR.000000000000134]
- 2 **Canto JG**, Shlipak MG, Rogers WJ, Malmgren JA, Frederick PD, Lambrew CT, Ornato JP, Barron HV, Kiefe CI. Prevalence, clinical characteristics, and mortality among patients with myocardial infarction presenting without chest pain. *JAMA* 2000; **283**: 3223-3229 [PMID: 10866870 DOI: 10.1001/jama.283.24.3223]
 - 3 **Kosuge M**, Kimura K, Ishikawa T, Ebina T, Hibi K, Tsukahara K, Kanna M, Iwahashi N, Okuda J, Nozawa N, Ozaki H, Yano H, Nakati T, Kusama I, Umemura S. Differences between men and women in terms of clinical features of ST-segment elevation acute myocardial infarction. *Circ J* 2006; **70**: 222-226 [PMID: 16501283 DOI: 10.1253/circj.70.222]
 - 4 **Body R**, Carley S, Wibberley C, McDowell G, Ferguson J, Mackway-Jones K. The value of symptoms and signs in the emergent diagnosis of acute coronary syndromes. *Resuscitation* 2010; **81**: 281-286 [PMID: 20036454 DOI: 10.1016/j.resuscitation.2009.11.014]
 - 5 **Larson DB**, Johnson LW, Schnell BM, Salisbury SR, Forman HP. National trends in CT use in the emergency department: 1995-2007. *Radiology* 2011; **258**: 164-173 [PMID: 21115875 DOI: 10.1148/radiol.10100640]
 - 6 **Shriki JE**, Shinbane J, Lee C, Khan AR, Burns N, Hindoyan A, Wilcox A. Incidental myocardial infarct on conventional nongated CT: a review of the spectrum of findings with gated CT and cardiac MRI correlation. *AJR Am J Roentgenol* 2012; **198**: 496-504 [PMID: 22357988 DOI: 10.2214/AJR.11.7683]
 - 7 **American College of Cardiology Foundation Task Force on Expert Consensus Documents**, Mark DB, Berman DS, Budoff MJ, Carr JJ, Gerber TC, Hecht HS, Hlatky MA, Hodgson JM, Lauer MS, Miller JM, Morin RL, Mukherjee D, Poon M, Rubin GD, Schwartz RS. ACCF/ACR/AHA/NASCI/SAIP/SCAI/SCCT 2010 expert consensus document on coronary computed tomographic angiography: a report of the American College of Cardiology Foundation Task Force on Expert Consensus Documents. *J Am Coll Cardiol* 2010; **55**: 2663-2699 [PMID: 20513611 DOI: 10.1016/j.jacc.2009.11.013]
 - 8 **Goldstein JA**, Chinnaiyan KM, Abidov A, Achenbach S, Berman DS, Hayes SW, Hoffmann U, Lesser JR, Mikati IA, O'Neil BJ, Shaw LJ, Shen MY, Valeti US, Raff GL; CT-STAT Investigators. The CT-STAT (Coronary Computed Tomographic Angiography for Systematic Triage of Acute Chest Pain Patients to Treatment) trial. *J Am Coll Cardiol* 2011; **58**: 1414-1422 [PMID: 21939822 DOI: 10.1016/j.jacc.2011.03.068]
 - 9 **Hoffmann U**, Truong QA, Schoenfeld DA, Chou ET, Woodard PK, Nagurney JT, Pope JH, Hauser TH, White CS, Weiner SG, Kalanjian S, Mullins ME, Mikati I, Peacock WF, Zakrofsky P, Hayden D, Goehler A, Lee H, Gazelle GS, Wiviott SD, Fleg JL, Udelson JE; ROMICAT-II Investigators. Coronary CT angiography vs standard evaluation in acute chest pain. *N Engl J Med* 2012; **367**: 299-308 [PMID: 22830462 DOI: 10.1056/NEJMoa1201161]
 - 10 **Litt HL**, Gatsonis C, Snyder B, Singh H, Miller CD, Entrikin DW, Leaming JM, Gavin LJ, Pacella CB, Hollander JE. CT angiography for safe discharge of patients with possible acute coronary syndromes. *N Engl J Med* 2012; **366**: 1393-1403 [PMID: 22449295 DOI: 10.1056/NEJMoa1201163]
 - 11 **Cury RC**, Feuchtner GM, Batlle JC, Peña CS, Janowitz W, Katzen BT, Ziffer JA. Triage of patients presenting with chest pain to the emergency department: implementation of coronary CT angiography in a large urban health care system. *AJR Am J Roentgenol* 2013; **200**: 57-65 [PMID: 23255742 DOI: 10.2214/AJR.12.8808]
 - 12 **Taylor AJ**, Cerqueira M, Hodgson JM, Mark D, Min J, O'Gara P, Rubin GD; American College of Cardiology Foundation Appropriate Use Criteria Task Force; Society of Cardiovascular Computed Tomography; American College of Radiology; American Heart Association; American Society of Echocardiography; American Society of Nuclear Cardiology; North American Society for Cardiovascular Imaging; Society for Cardiovascular Angiography and Interventions; Society for Cardiovascular Magnetic Resonance, Kramer CM, Berman D, Brown A, Chaudhry FA, Cury RC, Desai MY, Einstein AJ, Gomes AS, Harrington R, Hoffmann U, Khare R, Lesser J, McGann C, Rosenberg A, Schwartz R, Shelton M, Smetana GW, Smith SC Jr. ACCF/SCCT/ACR/AHA/ASE/ASNC/NASCI/SCAI/SCMR 2010 appropriate use criteria for cardiac computed tomography. A report of the American College of Cardiology Foundation Appropriate Use Criteria Task Force, the Society of Cardiovascular Computed Tomography, the American College of Radiology, the American Heart Association, the American Society of Echocardiography, the American Society of Nuclear Cardiology, the North American Society for Cardiovascular Imaging, the Society for Cardiovascular Angiography and Interventions, and the Society for Cardiovascular Magnetic Resonance. *J Am Coll Cardiol* 2010; **56**: 1864-1894 [PMID: 21087721 DOI: 10.1016/j.jacc.2010.07.005]
 - 13 **Pursnani A**, Lee AM, Mayrhofer T, Ahmed W, Uthamalingam S, Ferencik M, Puchner SB, Bamberg F, Schlett CL, Udelson J, Hoffmann U, Ghoshhajra BB. Early resting myocardial computed tomography perfusion for the detection of acute coronary syndrome in patients with coronary artery disease. *Circ Cardiovasc Imaging* 2015; **8**: e002404 [PMID: 25752898 DOI: 10.1161/CIRCIMAGING.114.002404]
 - 14 **Leipsic J**, Abbara S, Achenbach S, Cury R, Earls JP, Mancini GJ, Nieman K, Pontone G, Raff GL. SCCT guidelines for the interpretation and reporting of coronary CT angiography: a report of the Society of Cardiovascular Computed Tomography Guidelines Committee. *J Cardiovasc Comput Tomogr* 2014; **8**: 342-358 [PMID: 25301040 DOI: 10.1016/j.jcct.2014.07.003]
 - 15 **Gosalia A**, Haramati LB, Sheth MP, Spindola-Franco H. CT detection of acute myocardial infarction. *AJR Am J Roentgenol* 2004; **182**: 1563-1566 [PMID: 15150010 DOI: 10.2214/ajr.182.6.1821563]
 - 16 **Moore W**, Fields J, Mieczkowski B. Multidetector computed tomography pulmonary angiogram in the assessment of myocardial infarction. *J Comput Assist Tomogr* 2006; **30**: 800-803 [PMID: 16954933 DOI: 10.1097/01.rct.0000230001.15650.05]
 - 17 **Mano Y**, Anzai T, Yoshizawa A, Itabashi Y, Ohki T. Role of non-electrocardiogram-gated contrast-enhanced computed tomography in the diagnosis of acute coronary syndrome. *Heart Vessels* 2015; **30**: 1-8 [PMID: 24221182 DOI: 10.1007/s00380-013-0437-8]
 - 18 **Watanabe T**, Furuse Y, Ohta Y, Kato M, Ogawa T, Yamamoto K. The Effectiveness of Non-ECG-Gated Contrast-Enhanced Computed Tomography for the Diagnosis of Non-ST Segment Elevation Acute Coronary Syndrome. *Int Heart J* 2016; **57**: 558-564 [PMID: 27593539 DOI: 10.1536/ihj.16-072]
 - 19 **Yamazaki M**, Higuchi T, Shimokoshi T, Kiguchi T, Horii Y, Yoshimura N, Aoyama H. Acute coronary syndrome: evaluation of detection capability using non-electrocardiogram-gated parenchymal phase CT imaging. *Jpn J Radiol* 2016;

- 34: 331-338 [PMID: 26883335 DOI: 10.1007/s11604-016-0527-5]
- 20 **Cerqueira MD**, Weissman NJ, Dilsizian V, Jacobs AK, Kaul S, Laskey WK, Pennell DJ, Rumberger JA, Ryan T, Verani MS; American Heart Association Writing Group on Myocardial Segmentation and Registration for Cardiac Imaging. Standardized myocardial segmentation and nomenclature for tomographic imaging of the heart. A statement for healthcare professionals from the Cardiac Imaging Committee of the Council on Clinical Cardiology of the American Heart Association. *Circulation* 2002; **105**: 539-542 [PMID: 11815441 DOI: 10.1161/hc0402.102975]
 - 21 **Angelini P**. Coronary artery anomalies--current clinical issues: definitions, classification, incidence, clinical relevance, and treatment guidelines. *Tex Heart Inst J* 2002; **29**: 271-278 [PMID: 12484611]
 - 22 **Berman DS**, Kang X, Slomka PJ, Gerlach J, de Yang L, Hayes SW, Friedman JD, Thomson LE, Germano G. Underestimation of extent of ischemia by gated SPECT myocardial perfusion imaging in patients with left main coronary artery disease. *J Nucl Cardiol* 2007; **14**: 521-528 [PMID: 17679060 DOI: 10.1016/j.nuclcard.2007.05.008]
 - 23 **Wang ZJ**, Reddy GP, Gotway MB, Yeh BM, Hetts SW, Higgins CB. CT and MR imaging of pericardial disease. *Radiographics* 2003; **23** Spec No: S167-S180 [PMID: 14557510 DOI: 10.1148/rg.23si035504]
 - 24 **Haddadin S**, Milano AD, Faggian G, Morjan M, Patelli F, Golia G, Franchi P, Mazzucco A. Surgical treatment of postinfarction left ventricular free wall rupture. *J Card Surg* 2009; **24**: 624-631 [PMID: 20078707 DOI: 10.1111/j.1540-8191.2009.00896.x]
 - 25 **Restrepo CS**, Gutierrez FR, Marmol-Velez JA, Ocazonez D, Martinez-Jimenez S. Imaging patients with cardiac trauma. *Radiographics* 2012; **32**: 633-649 [PMID: 22582351 DOI: 10.1148/rg.323115123]
 - 26 **Otto CM**. Clinical practice. Evaluation and management of chronic mitral regurgitation. *N Engl J Med* 2001; **345**: 740-746 [PMID: 11547744 DOI: 10.1056/NEJMcp003331]
 - 27 **Voci P**, Bilotta F, Caretta Q, Mercanti C, Marino B. Papillary muscle perfusion pattern. A hypothesis for ischemic papillary muscle dysfunction. *Circulation* 1995; **91**: 1714-1718 [PMID: 7882478 DOI: 10.1161/01.cir.91.6.1714]
 - 28 **Nieman K**, Cury RC, Ferencik M, Nomura CH, Abbara S, Hoffmann U, Gold HK, Jang IK, Brady TJ. Differentiation of recent and chronic myocardial infarction by cardiac computed tomography. *Am J Cardiol* 2006; **98**: 303-308 [PMID: 16860013 DOI: 10.1016/j.amjcard.2006.01.101]
 - 29 **Baroldi G**, Silver MD, De Maria R, Parodi O, Pellegrini A. Lipomatous metaplasia in left ventricular scar. *Can J Cardiol* 1997; **13**: 65-71 [PMID: 9039067]
 - 30 **Su L**, Siegel JE, Fishbein MC. Adipose tissue in myocardial infarction. *Cardiovasc Pathol* 2004; **13**: 98-102 [PMID: 15033159 DOI: 10.1016/S1054-8807(03)00134-0]
 - 31 **Kimura F**, Matsuo Y, Nakajima T, Nishikawa T, Kawamura S, Sannohe S, Hagiwara N, Sakai F. Myocardial fat at cardiac imaging: how can we differentiate pathologic from physiologic fatty infiltration? *Radiographics* 2010; **30**: 1587-1602 [PMID: 21071377 DOI: 10.1148/rg.306105519]
 - 32 **Ichikawa Y**, Kitagawa K, Chino S, Ishida M, Matsuoka K, Tanigawa T, Nakamura T, Hirano T, Takeda K, Sakuma H. Adipose tissue detected by multislice computed tomography in patients after myocardial infarction. *JACC Cardiovasc Imaging* 2009; **2**: 548-555 [PMID: 19442939 DOI: 10.1016/j.jcmg.2009.01.010]

Diagnostic accuracy of thoracic imaging modalities for the detection of COVID-19

Haben Dawit, Marissa Absi, Nayaar Islam, Sanam Ebrahimzadeh, Matthew D F McInnes

Specialty type: Radiology, nuclear medicine and medical imaging

Provenance and peer review: Unsolicited article; Externally peer reviewed.

Peer-review model: Single blind

Peer-review report's scientific quality classification

Grade A (Excellent): A
Grade B (Very good): 0
Grade C (Good): 0
Grade D (Fair): 0
Grade E (Poor): 0

P-Reviewer: Sageena G

Received: August 7, 2021

Peer-review started: August 7, 2021

First decision: November 11, 2021

Revised: November 11, 2021

Accepted: February 19, 2022

Article in press: February 19, 2022

Published online: February 28, 2022



Haben Dawit, Marissa Absi, Nayaar Islam, Sanam Ebrahimzadeh, Clinical Epidemiology Program, Ottawa Hospital Research Institute, Ottawa K1E4M9, ON, Canada

Matthew D F McInnes, Department of Radiology, The Ottawa Hospital Research Institute Clinical Epidemiology Program, Ottawa K1H8L6, ON, Canada

Corresponding author: Matthew D F McInnes, MD, PhD, Professor, Department of Radiology, The Ottawa Hospital Research Institute Clinical Epidemiology Program, 451 Smyth Road, Ottawa K1H8L6, ON, Canada. mmcinnnes@toh.ca

Abstract

The ongoing coronavirus disease 2019 (COVID-19) pandemic continues to present diagnostic challenges. The use of thoracic radiography has been studied as a method to improve the diagnostic accuracy of COVID-19. The 'Living' Cochrane Systematic Review on the diagnostic accuracy of imaging tests for COVID-19 is continuously updated as new information becomes available for study. In the most recent version, published in March 2021, a meta-analysis was done to determine the pooled sensitivity and specificity of chest X-ray (CXR) and lung ultrasound (LUS) for the diagnosis of COVID-19. CXR gave a sensitivity of 80.6% (95%CI: 69.1-88.6) and a specificity of 71.5% (95%CI: 59.8-80.8). LUS gave a sensitivity rate of 86.4% (95%CI: 72.7-93.9) and specificity of 54.6% (95%CI: 35.3-72.6). These results differed from the findings reported in the recent article in this journal where they cited the previous versions of the study in which a meta-analysis for CXR and LUS could not be performed. Additionally, the article states that COVID-19 could not be distinguished, using chest computed tomography (CT), from other respiratory diseases. However, the latest review version identifies chest CT as having a specificity of 80.0% (95%CI: 74.9-84.3), which is much higher than the previous version which indicated a specificity of 61.1% (95%CI: 42.3-77.1). Therefore, CXR, chest CT and LUS have the potential to be used in conjunction with other methods in the diagnosis of COVID-19.

Key Words: COVID-19; Chest x-ray; Computed tomography; Lung ultrasound; Specificity and sensitivity; Diagnostic accuracy

©The Author(s) 2022. Published by Baishideng Publishing Group Inc. All rights reserved.

Core Tip: The global coronavirus disease 2019 (COVID-19) outbreak has greatly impacted the world, with almost 200 million cases worldwide and more than 4 million deaths (as of July 21, 2021). Reverse transcriptase polymerase chain reaction is the current gold-standard for diagnosing COVID-19, but due to a diagnostic error rate greater than 10%, alternate modes of diagnosis are needed. Our review demonstrates that chest X-ray, chest computed tomography and lung ultrasound may have the potential to aid healthcare workers in the diagnosis of COVID-19.

Citation: Dawit H, Absi M, Islam N, Ebrahimzadeh S, McInnes MDF. Diagnostic accuracy of thoracic imaging modalities for the detection of COVID-19. *World J Radiol* 2022; 14(2): 47-49

URL: <https://www.wjgnet.com/1949-8470/full/v14/i2/47.htm>

DOI: <https://dx.doi.org/10.4329/wjr.v14.i2.47>

TO THE EDITOR

We appreciate Kumar *et al*[1] consideration of our study in their paper on the discrepancies in the clinical and radiological profiles of coronavirus disease 2019 (COVID-19)[1]. In this paper, the use of chest computed tomography (CT), chest X-ray (CXR), and lung ultrasound (LUS) as possible diagnostic tools for the COVID-19 is discussed. The authors cite the findings from two versions of the Cochrane Review titled “Thoracic imaging tests for the diagnosis of COVID-19.” As more information becomes available, this systematic review has aimed to keep pace with the new data. The most recent version of the review, published in March 2021, has shown differences in the sensitivities and specificities of these three image modalities compared to the findings in prior versions reported in the article by Kumar *et al* [1].

Firstly, the authors cited the initial review by Salameh *et al*[2], which determined that CXR had a pooled sensitivity of CXR is 82.1% (95%CI: 62.5-92.7)[1,2] in patients who had COVID-19. The second version of the review, by Islam *et al*[3], determined that CXR had a sensitivity ranging from 56.9% to 89.0% and specificity ranging from 11.1% to 88.9%[1,3] in patients with COVID-19. As opposed to the first two versions, in the third and most recent version, there was a sufficient number of studies, evaluating the diagnostic accuracy of CXR, to perform a meta-analysis. The updated version of the review conducted a meta-analysis with 9 studies and 3694 participants for CXR. The following imaging modality had sensitivity and specificity of 80.6% (95%CI: 69.1-88.6) and 71.5% (95%CI: 59.8-80.8)[4], respectively. These findings demonstrate that CXR is moderately sensitive and moderately specific to COVID-19, and may have the potential to be used as a secondary method for diagnosis, however, due to the limited number of studies, accuracy estimates must be carefully interpreted[4]. In the upcoming fourth version of the systematic review, additional studies evaluating CXR have been included. In this review, additional analyses have been done to support our conclusion, and potential sources of variabilities in CXR accuracy estimates will be discussed.

Secondly, the article by Kumar *et al*[1] states that chest CT may not be capable of discriminating COVID-19 from other respiratory diseases[1]. The review by Salameh *et al*[2] obtained a pooled specificity of 18.1% (95%CI: 3.71-55.8)[2] for chest CT, in cases where CT scans were used as the primary diagnostic test, which was subsequently updated to 61.1% (95%CI: 42.3-77.1) in the subsequent edition [3]. The third and most recent version identified that the specificity of chest CT has increased substantially to 80.0% (95%CI: 74.9-84.3), based on 41 studies with 16133 patients[4]. The improved specificity could be due to the stricter inclusion criteria for this version. In the most recent version, studies that published index test findings without clearly defining the images as positive or negative[4] for COVID-19, were excluded. An alternate explanation for the improved specificity could be the increase in studies that use well-developed definitions for index test positivity (*e.g.* Co-RADS)[4]. Furthermore, studies from the later stage of the pandemic were included with each review version which affected our specificity values through improved knowledge about the indications of COVID-19 in imaging results [4].

Lastly, the most recent version of the ‘Living’ Cochrane Systematic Review observed that in patients suspected of having COVID-19, LUS had a sensitivity and specificity rate of 86.4% (95%CI: 72.7-93.9) and 54.6% (95%CI: 35.3-72.6)[4], respectively. The accuracy estimates were produced through a meta-analysis including 5 studies with 446 patients[4]. These findings differ from the second review version cited by Kumar *et al*[1], which reported a sensitivity of 96.8% and sensitivity of 62.3% for LUS[1,3]. The second version of the review was based off of one study, therefore a meta-analysis was not completed[1, 3]. The increase in studies in the most recent version reduced the role of chance in our results, and provided a better picture of the diagnostic accuracy of LUS; however, the number of studies remains small and all data should be carefully interpreted.

In summary, the most recent version of the ‘Living’ Cochrane Systematic Review was able to perform further analyses on the diagnostic accuracy of CXR and LUS. The data demonstrates that CXR is moderately specific and moderately sensitive, while LUS is sensitive, but not specific for the diagnosis

of COVID-19. Additionally, the review demonstrated that chest CT is moderately specific for the diagnosis of COVID-19. We hope that future studies will be more rigorous and transparent when designing and reporting the findings of their study. We admire the continued interest in our systematic review and will update our review as more information on the diagnostic accuracy of these imaging modalities becomes available.

FOOTNOTES

Author contributions: All authors contributed to writing and editing this work.

Conflict-of-interest statement: There was no conflict of interest present in the production of this letter.

Open-Access: This article is an open-access article that was selected by an in-house editor and fully peer-reviewed by external reviewers. It is distributed in accordance with the Creative Commons Attribution NonCommercial (CC BY-NC 4.0) license, which permits others to distribute, remix, adapt, build upon this work non-commercially, and license their derivative works on different terms, provided the original work is properly cited and the use is non-commercial. See: <https://creativecommons.org/licenses/by-nc/4.0/>

Country/Territory of origin: Canada

ORCID number: Haben Dawit 0000-0002-8052-4124; Marissa Absi 0000-0003-4581-9629; Nayaar Islam 0000-0002-1159-7629; Sanam Ebrahimzadeh 0000-0003-3890-1683; Matthew D F McInnes 0000-0001-8404-4075.

S-Editor: Fan JR

L-Editor: A

P-Editor: Fan JR

REFERENCES

- 1 **Kumar H**, Fernandez CJ, Kolpattil S, Munavvar M, Pappachan JM. Discrepancies in the clinical and radiological profiles of COVID-19: A case-based discussion and review of literature. *World J Radiol* 2021; **13**: 75-93 [PMID: 33968311 DOI: 10.4329/wjr.v13.i4.75]
- 2 **Salameh JP**, Leeftang MM, Hooft L, Islam N, McGrath TA, van der Pol CB, Frank RA, Prager R, Hare SS, Dennie C, Spijker R, Deeks JJ, Dinnes J, Jenniskens K, Korevaar DA, Cohen JF, Van den Bruel A, Takwoingi Y, van de Wijgert J, Damen JA, Wang J; Cochrane COVID-19 Diagnostic Test Accuracy Group, McInnes MD. Thoracic imaging tests for the diagnosis of COVID-19. *Cochrane Database Syst Rev* 2020; **9**: CD013639 [PMID: 32997361 DOI: 10.1002/14651858.CD013639.pub2]
- 3 **Islam N**, Salameh JP, Leeftang MM, Hooft L, McGrath TA, van der Pol CB, Frank RA, Kazi S, Prager R, Hare SS, Dennie C, Spijker R, Deeks JJ, Dinnes J, Jenniskens K, Korevaar DA, Cohen JF, Van den Bruel A, Takwoingi Y, van de Wijgert J, Wang J, McInnes MD; Cochrane COVID-19 Diagnostic Test Accuracy Group. Thoracic imaging tests for the diagnosis of COVID-19. *Cochrane Database Syst Rev* 2020; **11**: CD013639 [PMID: 33242342 DOI: 10.1002/14651858.CD013639.pub3]
- 4 **Islam N**, Ebrahimzadeh S, Salameh JP, Kazi S, Fabiano N, Treanor L, Absi M, Hallgrimson Z, Leeftang MM, Hooft L, van der Pol CB, Prager R, Hare SS, Dennie C, Spijker R, Deeks JJ, Dinnes J, Jenniskens K, Korevaar DA, Cohen JF, Van den Bruel A, Takwoingi Y, van de Wijgert J, Damen JA, Wang J, McInnes MD; Cochrane COVID-19 Diagnostic Test Accuracy Group. Thoracic imaging tests for the diagnosis of COVID-19. *Cochrane Database Syst Rev* 2021; **3**: CD013639 [PMID: 33724443 DOI: 10.1002/14651858.CD013639.pub4]

Comments on "Review of the role of diagnostic modalities and imaging findings in the COVID-19 pandemic"

Sai Swarupa R Vulasala, Dheeraj R Gopireddy, Priya Bhosale, Mayur K Virarkar

Specialty type: Radiology, nuclear medicine and medical imaging

Provenance and peer review: Invited article; Externally peer reviewed.

Peer-review model: Single blind

Peer-review report's scientific quality classification

Grade A (Excellent): 0
Grade B (Very good): B, B, B
Grade C (Good): 0
Grade D (Fair): 0
Grade E (Poor): 0

P-Reviewer: Al-Ani RM, Samadder S, Shariati MBH

Received: November 6, 2021

Peer-review started: November 6, 2021

First decision: December 10, 2021

Revised: December 11, 2021

Accepted: February 15, 2022

Article in press: February 15, 2022

Published online: February 28, 2022



Sai Swarupa R Vulasala, Dheeraj R Gopireddy, Mayur K Virarkar, Department of Radiology, University of Florida College of Medicine, Jacksonville, FL 32209, United States

Priya Bhosale, Department of Diagnostic Radiology, UT MD Anderson Cancer Center, Houston, TX 77030, United States

Corresponding author: Sai Swarupa R Vulasala, MBBS, Research Assistant, Radiology, University of Florida College of Medicine, No. 655 West 8th Street, C90 2nd Floor, Clinical Center, Jacksonville, FL 32209, United States. vulasalaswarupa@gmail.com

Abstract

The present letter to the editor corresponds to the article entitled "Comprehensive literature review on the radiographic findings, imaging modalities, and the role of radiology in the coronavirus disease 2019 (COVID-19) pandemic" by Pal *et al*, published in *World J Radiol.* 2021; 13(9): 258-282. With zero to unknown prevalence, COVID-19 has created a heterogeneous and unforeseen situation across the world. Healthcare providers encountered new challenges in image interpretation, characterization, and prognostication of the disease. Pal *et al* delineated the radiological findings, which would guide the radiologists to identify the early signs of severe infection.

Key Words: COVID-19; Computed tomography; Lung ultrasound; COVID-19 scoring systems

©The Author(s) 2022. Published by Baishideng Publishing Group Inc. All rights reserved.

Core Tip: Besides reverse transcriptase-polymerase chain reaction being the most standard test, chest X-ray, computed tomography, and lung ultrasound play a supportive role for Coronavirus disease 2019 (COVID-19) diagnosis. The main focus of this letter is to emphasize the importance of imaging in the COVID-19 pandemic. The various imaging characteristics aid in determining the severity of the disease and prognosis. The implementation of scoring systems further improves diagnostic efficiency. In addition, Pal *et al* discussed their COVID-19 first wave experience and recommended a few strategies for overcoming the second wave.

Citation: Vulasala SSR, Gopireddy DR, Bhosale P, Virarkar MK. Comments on "Review of the role of diagnostic modalities and imaging findings in the COVID-19 pandemic". *World J Radiol* 2022; 14(2): 50-54

URL: <https://www.wjgnet.com/1949-8470/full/v14/i2/50.htm>

DOI: <https://dx.doi.org/10.4329/wjr.v14.i2.50>

TO THE EDITOR

We read with interest the article published in the World Journal of Radiology by Pal *et al*[1] on the depiction of radiological findings in identifying and predicting coronavirus disease 2019 (COVID-19) patient patterns. We would like to commend the authors for this vital article encompassing the pathophysiology and evidence-based review of COVID-19 severity scoring systems on chest X-ray (CXR), computed tomography (CT), and lung ultrasound (LUS). The authors outlined the artificial intelligence (AI) aspect of the diagnostic process and its importance in supporting human resources during the pandemic.

Although reverse transcriptase-polymerase chain reaction (RT-PCR) is the standard work-up for a specific diagnosis, it is limited by sample quality, laboratory errors, ribonucleic acid (RNA) stability, and variable sensitivity[2]. RT-PCR involves two steps: (1) Reverse transcription; and (2) Quantitative real time polymerase chain reaction. It can detect RNA by using either RNA or deoxyribonucleic acid (DNA) as positive controls. Most of the commercial kits adopt DNA as control in fear of RNA degradation by ribonucleases (RNases). However, DNA kits cannot report failed reverse transcriptase step, thus resulting in high false negative rates (40%) and variable sensitivity[3]. To avoid this concern, appropriate controls are necessary for viral RNA detection. Also, a negative RT-PCR requires repetition of the test in cases of clinical suspicion[4]. In contrast, imaging is a rapid and reliable procedure to evaluate suspicion of COVID-19 in individuals presenting with cough, dyspnea, and fatigue. At the beginning of the pandemic, there was a distinct and contentious discussion on the role and importance of radiology as part of the clinical management of COVID-19.

CXR is a readily accessible and inexpensive modality in the majority of clinical settings. It is helpful for triage among suspected COVID-19 individuals in the emergency department[5]. Peripheral predominant hazy opacification, bilateral lower lobe consolidation, and air space opacities similar to acute respiratory distress syndrome are the characteristic findings of COVID-19 on CXR. Pleural effusion, nodules, and pneumothorax are also unusual findings that can be discerned in COVID-19 patients[6].

Radiological assessment of lung edema (RALE) (Table 1) and Brixia score (Table 2) are the CXR-based grading systems in practice to predict the severity and prognosis of COVID-19 disease. According to a study by Au-Yong *et al*[7], RALE and Brixia scores have correlations of 0.87 and 0.86, respectively, in predicting patient outcomes. Individuals with high scores (RALE > 25 and Brixia > 11) have increased chances of intensive care unit admission or death within 60 days after diagnosis. As acknowledged by Pal *et al*[1] the usage of CXR has been limited by lower sensitivity (56%) and specificity (60%).

CT imaging is the preferred diagnostic modality, given its high sensitivity (94%)[1]. However, the specificity of CT ranges from 25% to 80%[1]. Lateralized, bilateral, multifocal, basilar and peripheral predominance and peripheral ground-glass opacities are the classical CT findings of COVID-19 pneumonia. Non-classical features include subsegmental vessel engorgement, "atoll sign," reticular opacifications, subpleural curvilinear opacifications, and bilateral hilar lymphadenopathy. All these findings are well illustrated by Pal *et al*[1].

COVID-19 reporting and data system (CO-RADS) (Table 3) and MuLBSTA (multilobular infiltration, hypo-lymphocytosis, bacterial coinfection, smoking history, hypertension, and age) (Table 4) scoring systems aid in the identification of the lung involvement and prognosis in suspected COVID-19 patients. Pal *et al*[1] described that CO-RADS and MuLBSTA have a sensitivity of 61% and 65.1%, and specificity of 81% and 95.4%, respectively. The main drawbacks of CT in clinical setting are: radiation exposure, the need to transfer the patient to the imaging room, and availability.

Lung ultrasound (LUS) may assist physicians in assessing the disease severity with sensitivity and specificity of 65%-76.9% and 72.7%-77.1%, respectively[1]. It identifies subtle lung findings in the periphery which remain hidden in majority of CXR[8]. In addition, the findings of COVID-19 pneumonia on LUS correlate well with CT findings[9,10]. Hence LUS can be employed in the common and standard practice. LUS is advantageous as it eliminates the radiation risk and resource consumption of CXR and CT, if the patients require daily monitoring of lung status. It also overcomes the limitations of CT by its portability and accessibility at bedside with great learning curve. B-line artifacts, subpleural consolidations, pleural irregularities, and patchy opacities can be seen on the LUS of COVID-19-infected patients. The presence of B-lines indicates parenchymal involvement, and they increase proportionately with the disease, resulting in "white lungs"[2]. With recuperation from illness, B-lines are replaced with A-lines, which represent normal lung surface. Subpleural consolidation specifies the inflammatory changes; however, these findings may last for several weeks after recovery.

Table 1 Radiological assessment of lung edema classification[13]

Consolidation	
Score	Extent of alveolar opacities in each lung quadrant.
0	0%
1	0-25%
2	25-50%
3	50-75%
4	> 75%
If consolidation is ≥ 1, then score density	
1	Hazy
2	Moderate
3	Dense
Final RALE scoring	
Right lung	Left lung
Upper quadrant, Cons × Density= Q1	Upper quadrant, Cons × Density= Q3
Lower quadrant, Cons × Density= Q2	Lower quadrant, Cons × Density= Q4
Total RALE: Q1+Q2+Q3+Q4	

RALE: Radiological assessment of lung edema.

Table 2 Brixia score

Score	Findings on CXR in three divided zones of each lung
0	No abnormal findings
1	Interstitial infiltrates
2	Interstitial > Alveolar infiltrates
3	Alveolar > Interstitial infiltrates

CXR: Chest X-ray.

A 12-zone scoring system is used to quantify and predict the severity of lung involvement. Individuals are classified as normal, mild, moderate, and severely infected, with scores of 0, 1-5, 6-14, and ≥ 15, respectively. A cutoff score of 8 of 36 is 91% sensitive in predicting COVID-19 diagnosis. Hence LUS may be used as a screening tool, but in conjunction with other imaging modalities due to its ineffective differentiation between acute ongoing infection and recovery[1,2].

Although the role of magnetic resonance imaging, Fluorodeoxyglucose positron emission tomography, CT pulmonary angiography, and point-of-care echocardiography is limited in COVID-19, they may help detect complications such as myocarditis, cardiomyopathy, right ventricular dilatation, and pulmonary embolism and monitor the treatment response. AI is an algorithm-based entity that allows rapid diagnosis and enhances a health system’s capability. AI COVID-19 algorithm has a sensitivity, specificity, and accuracy of 84%, 93%, and 90.8%, respectively. AI-based deep learning technology has detected COVID-19 on CT with an area under the receiver operating characteristic curve of 0.96 and sensitivity and specificity of 90% and 96%, respectively[11]. Wehbe *et al*[12] compared the performance of AI and radiologists and reported similar diagnostic accuracy of 82% and 81%, respectively. Hence, AI has the ability to assist radiologists in prompt diagnosis and to improve workflow efficiency.

Familiarity with the COVID-19 imaging findings was essential for radiologists working during the pandemic. Even though the disease spread is controlled currently, the discovery of newer virus strains highlights the importance of strategies such as increasing work capacity and imaging capabilities that might be helpful during a future unanticipated outbreak.

Table 3 Coronavirus disease 2019 reporting and data system classification.

Category	Level of COVID-19 suspicion	Findings
0	Non-interpretable	Technically insufficient scan to assign a score
1	Very low	Normal lung
2	Low	Typical of infection other than COVID-19
3	Equivalent/ unsure	Non-specific findings to COVID-19 and other infections
4	High	Suspicious of COVID-19
5	Very high	Typical COVID-19 findings
6	Proven	Positive RT-PCR for COVID-19

COVID-19: Coronavirus disease 2019; RT-PCR: Reverse transcriptase- polymerase chain reaction.

Table 4 Multilobar infiltration, hypo-lymphocytosis, bacterial coinfection, smoking history, hypertension, and age scoring system

Parameter	Yes	No
Multi-lobar involvement	+ 5	0
Lymphopenia ($\leq 0.8 \times 10^9/L$)	+ 4	0
Bacterial co-infection in blood or sputum	+ 4	0
Smoking history	Active smoker: + 3; Prior Smoker: + 2	0
Hypertension	+ 2	0
Age ≥ 60 yr	+ 2	0

FOOTNOTES

Author contributions: Vulasala SSR, Gopireddy DR, Bhosale P, Virarkar MK have equal contributions; all authors have read and approved the final manuscript.

Conflict-of-interest statement: The authors declare they have no conflicts of interest.

Open-Access: This article is an open-access article that was selected by an in-house editor and fully peer-reviewed by external reviewers. It is distributed in accordance with the Creative Commons Attribution NonCommercial (CC BY-NC 4.0) license, which permits others to distribute, remix, adapt, build upon this work non-commercially, and license their derivative works on different terms, provided the original work is properly cited and the use is non-commercial. See: <https://creativecommons.org/licenses/by-nc/4.0/>

Country/Territory of origin: United States

ORCID number: Sai Swarupa R Vulasala 0000-0002-9387-3673; Dheeraj R Gopireddy 0000-0001-8441-7804; Priya Bhosale 0000-0003-4014-4941; Mayur K Virarkar 0000-0002-5825-3102.

S-Editor: Xing YX

L-Editor: A

P-Editor: Xing YX

REFERENCES

- 1 **Pal A, Ali A, Young TR, Oostenbrink J, Prabhakar A, Deacon N, Arnold A, Eltayeb A, Yap C, Young DM, Tang A, Lakshmanan S, Lim YY, Pokarowski M, Kakodkar P.** Comprehensive literature review on the radiographic findings, imaging modalities, and the role of radiology in the COVID-19 pandemic. *World J Radiol* 2021; **13**: 258-282 [PMID: 34630913 DOI: 10.4329/wjr.v13.i9.258]
- 2 **Skoczyński S, Buda N, Mendrala K, Górecki T, Kucewicz-Czech E, Krzych Ł, Koszutski T, Darocha T.** Lung ultrasound may improve COVID-19 safety protocols. *J Thorac Dis* 2021; **13**: 2698-2704 [PMID: 34164162 DOI: 10.21037/jtd-21-295]
- 3 **Luo G, Zhang J, Zhang S, Hu B, Hu L, Huang Z.** High-quality RT-PCR with chemically modified RNA controls. *Talanta* 2021; **224**: 121850 [PMID: 33379066 DOI: 10.1016/j.talanta.2020.121850]

- 4 **Arevalo-Rodriguez I**, Buitrago-Garcia D, Simancas-Racines D, Zambrano-Achig P, Del Campo R, Ciapponi A, Sued O, Martinez-García L, Rutjes AW, Low N, Bossuyt PM, Perez-Molina JA, Zamora J. False-negative results of initial RT-PCR assays for COVID-19: A systematic review. *PLoS One* 2020; **15**: e0242958 [PMID: [33301459](#) DOI: [10.1371/journal.pone.0242958](#)]
- 5 **Reeves RA**, Pomeranz C, Gomella AA, Gulati A, Metra B, Hage AN, Lange S, Parekh M, Donuru A, Lakhani P, Sundaram B. Performance of a Severity Score on Admission Chest Radiography in Predicting Clinical Outcomes in Hospitalized Patients With Coronavirus Disease (COVID-19). *AJR Am J Roentgenol* 2021; **217**: 623-632 [PMID: [33112201](#) DOI: [10.2214/AJR.20.24801](#)]
- 6 **Jacobi A**, Chung M, Bernheim A, Eber C. Portable chest X-ray in coronavirus disease-19 (COVID-19): A pictorial review. *Clin Imaging* 2020; **64**: 35-42 [PMID: [32302927](#) DOI: [10.1016/j.clinimag.2020.04.001](#)]
- 7 **Au-Yong I**, Higashi Y, Giannotti E, Fogarty A, Morling JR, Grainge M, Race A, Juurlink I, Simmonds M, Briggs S, Cruikshank S, Hammond-Pears S, West J, Crooks CJ, Card T. Chest Radiograph Scoring Alone or Combined with Other Risk Scores for Predicting Outcomes in COVID-19. *Radiology* 2021; 210986 [PMID: [34519573](#) DOI: [10.1148/radiol.2021210986](#)]
- 8 **Boero E**, Schreiber A, Rovida S, Vetrugno L, Blaivas M. The role of lung ultrasonography in COVID-19 disease management. *J Am Coll Emerg Physicians Open* 2020 [PMID: [32838389](#) DOI: [10.1002/emp2.12194](#)]
- 9 **Skopljanac I**, Ivelja MP, Barcot O, Brdar I, Dolic K, Polasek O, Radic M. Role of Lung Ultrasound in Predicting Clinical Severity and Fatality in COVID-19 Pneumonia. *J Pers Med* 2021; **11** [PMID: [34442401](#) DOI: [10.3390/jpm11080757](#)]
- 10 **Lieveld AWE**, Kok B, Azijli K, Schuit FH, van de Ven PM, de Korte CL, Nijveldt R, van den Heuvel FMA, Teunissen BP, Hoefsloot W, Nanayakkara PWB, Bosch FH. Assessing COVID-19 pneumonia-Clinical extension and risk with point-of-care ultrasound: A multicenter, prospective, observational study. *J Am Coll Emerg Physicians Open* 2021; **2**: e12429 [PMID: [33969350](#) DOI: [10.1002/emp2.12429](#)]
- 11 **Szabó IV**, Simon J, Nardocci C, Kardos AS, Nagy N, Abdelrahman RH, Zsarnóczay E, Fejér B, Futácsi B, Müller V, Merkely B, Maurovich-Horvat P. The Predictive Role of Artificial Intelligence-Based Chest CT Quantification in Patients with COVID-19 Pneumonia. *Tomography* 2021; **7**: 697-710 [PMID: [34842822](#) DOI: [10.3390/tomography7040058](#)]
- 12 **Wehbe RM**, Sheng J, Dutta S, Chai S, Dravid A, Barutcu S, Wu Y, Cantrell DR, Xiao N, Allen BD, MacNealy GA, Savas H, Agrawal R, Parekh N, Katsaggelos AK. DeepCOVID-XR: An Artificial Intelligence Algorithm to Detect COVID-19 on Chest Radiographs Trained and Tested on a Large U.S. Clinical Data Set. *Radiology* 2021; **299**: E167-E176 [PMID: [33231531](#) DOI: [10.1148/radiol.2020203511](#)]
- 13 **Warren MA**, Zhao Z, Koyama T, Bastarache JA, Shaver CM, Semler MW, Rice TW, Matthay MA, Calfee CS, Ware LB. Severity scoring of lung oedema on the chest radiograph is associated with clinical outcomes in ARDS. *Thorax* 2018; **73**: 840-846 [PMID: [29903755](#) DOI: [10.1136/thoraxjnl-2017-211280](#)]



Published by **Baishideng Publishing Group Inc**
7041 Koll Center Parkway, Suite 160, Pleasanton, CA 94566, USA

Telephone: +1-925-3991568

E-mail: bpgoffice@wjgnet.com

Help Desk: <https://www.f6publishing.com/helpdesk>

<https://www.wjgnet.com>

